Powder Technology 418 (2023) 118323

Contents lists available at ScienceDirect

Powder Technology

journal homepage: www.journals.elsevier.com/powder-technology

Contact force models for non-spherical particles with different surface properties: A review

Kamyar Kildashti [a], Kejun Dong [a,*], Aibing Yu [b]

[a] Centre for Infrastructure Engineering, School of Engineering, Design and Built Environment, Western Sydney University, NSW 2751, Australia
[b] ARC Hub for Computational Particle Technology, Department of Chemical Engineering, Monash University, Clayton, VIC 3800, Australia

HIGHLIGHTS

- Sophisticated contact force models for non-spherical particles reviewed.
- Accurate calculation of contact area and surface adhesion and asperity discussed.
- Models combined to calculate non-spherical particles with surface properties.
- Results from advanced models and simplified models are much different.
- A set of revised equations proposed for contact force calculation in DEM.

GRAPHICAL ABSTRACT

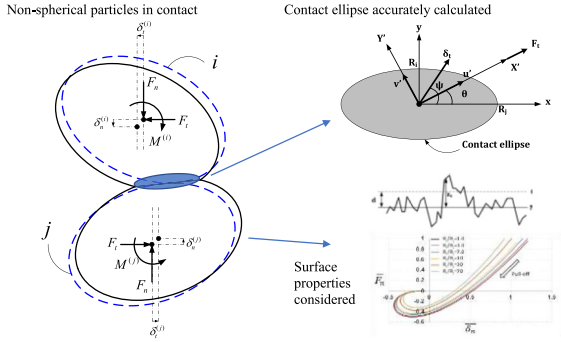

ARTICLE INFO

Keywords:
Discrete element method
Contact mechanics
Non-spherical particles
Contact force model

ABSTRACT

This paper reviews the state-of-the-art contact force models for non-spherical particles, which describe the relationship between the contact force and the geometrical, material, and mechanical properties of the contacting particles. The review aims to select better contact force models to improve the current simplified contact force models used in discrete element method (DEM) simulations. First, the contact force models based on the extension of the classical Hertz theory are reviewed, in which a recent accurate geometrical contact force model is highlighted. Secondly, the research on the effects of different variables such as elastoplasticity, viscoelasticity, adhesion and surface roughness on contact force are reviewed respectively and then incorporated into the accurate geometrical contact force model. Thirdly, tangential force models for non-spherical particles in contact under various loading regimes are reviewed as well. Based on the review, a full set of improved contact force models for DEM is recommended. These contact force models can more accurately predict the contact force and contact area for non-spherical particles, which can be beneficial to the DEM simulation in emerging areas, such as nanoparticles and additive manufacturing.

* Corresponding author.
E-mail address: kejun.dong@westernsydney.edu.au (K. Dong).

https://doi.org/10.1016/j.powtec.2023.118323
Received 19 December 2022; Received in revised form 1 February 2023; Accepted 2 February 2023
Available online 7 February 2023

Nomenclature

A	contact area of the summit of the asperity being described by either Hertzian or JKR theory
A_n	nominal contact area
A_{n-EP}	contact area in the elastic-plastic regime
A_p	contact area corresponding to fully plastic regime
E_i	Young's modulus of particles in touch
$\widehat{E}_c$	composite Young's modulus
E_d	frictional dissipated energy in each cycle
$\mathbb{E}(e^2)$	complete elliptic integral of the second kind
$\mathbf{F}_\mathrm{n}$	normal force vector
$\|\mathbf{F}_\mathrm{n}\|$	magnitude of normal force in the direction of normal vector **n**
F_{n0}	initial normal force
F_{n-EP}	contact normal load in the elastic-plastic regime
$\mathbf{F}_{\mathbf{n-dis}}$	dissipative normal contact force
F_{n-P}	fully plastic normal contact force
$\mathbf{F}_{\mathrm{n-V}}$	elastic plus viscoelastic normal contact force
F_t	tangential contact force
G	modulus of rigidity
$\widehat{G}$	composite shear modulus
H	hardness of the softer material in contact
$\mathbf{H}^n_{uv}$	Hessian Matrix
$\mathscr{I}_\vartheta(z)$	modified Bessel function of the first kind.
K_M	mean curvature
K_G	Gaussian curvature
$\mathbb{K}(e^2)$	complete elliptic integral of the first kind
$\mathscr{K}_\vartheta(z)$	modified Bessel function of the second kind
M_t	twisting couple
N	asperity density (the number of asperities per unit area)
R	radius of the shadow spherical potential particle being defined to satisfy strictly convex condition
R_i and R_j	effective radii of curvatures in the principal direction
$\widehat{R}_c$	effective radius of contact
$\Re$	elliptic tangential to the normal contact compliance
$(\mathbf{T_{1\mathit{I}}})_{\mathbf{def}}$, $(\mathbf{T_{1\mathit{II}}})_{\mathbf{def}}$	principal directions in default Cartesian frame for particles I and II
$W(A)$	contact energy potential of overlap area (A)
a, b, and c	half-lengths of an arbitrary super-quadric surface along principal axis
a_i, b_i,c_i, and d_i	parameters to approximate the potential particle faces with planes
a_c, b_c	major and minor semi-axis contact ellipse
a_{c0}	major semi-axis contact ellipse developed under F_{n0}
c_A	contact area constant
c_h	hardness coefficient for the fully plastic regime
c_{ij}	creepage and spin constants of proportionality
d	the separation distances
erf(x)	complementary error function
e^2	elliptical contact eccentricity
f	contact force of the summit of the asperity being described by either Hertzian or JKR theory
h	standardised separation
k	a coefficient determining the curvature of the faces of the final potential particle
k_n	the penalty coefficient
$\mathbf{n}$	vector of normal force acting on contact plane
$\mathbf{u}^t = (\mathscr{u}_x, \mathscr{u}_y, \mathscr{u}_z)^t$, $\mathbf{v}^t = (\mathscr{v}_x, \mathscr{v}_y, \mathscr{v}_z)^t$	arbitrary orthogonal unit vectors in tangent contact plane
r	distance by which the potential particle is expanded and related to the radius of curvature at corners
$\mathbf{x}_p = \{\mathrm{x}_p, \mathrm{y}_p\}$	cartesian coordinates of vertex p
z_s	asperity height measured from the mean line of the summit height
$\mathit{\Gamma} = 0$	equation, specifying the profile of the particle surface, either particle I or II
$\mathit{\Gamma}_\backslash$	gradient vector magnitude
Π_1 and Π_2	dimensionless quantities, taking the effects of contact adhesion energy into account
Φ	constant factor accounting elliptic contact area for tangential contact
$\nabla_{\mathbf{x}_p} A$	gradient of A with respect to $\mathbf{x}_p$
β	contact area correction factor to convert circular contact area to elliptical contact area
$\beta_{GW}{}^*$	contact area correction factor for GW rough contact
δ_n	contact normal overlap
$\dot{\delta}_n$	rate of normal overlap
δ_{n1}	critical normal overlap (the overlap corresponding to the yielding contact pressure)
δ_{n2}	onset of fully plastic normal contact overlap (elastic-plastic regime to fully plastic regime)
δ_t	relative tangential displacement of two mass central points
γ	contact force correction factor to convert circular contact area to elliptical contact area
$\gamma_{GW}{}^*$	contact force correction factor for GW rough contact
η_1, η_2	blockiness parameters for a super-quadric particle
η_{1i} and η_{2i}	coefficient of viscosity corresponding to bulk and shear deformation, respectively
θ	rotational angle with respect to the original position
θ_t	twisting angle of rotation
$\kappa_{1\mathit{I}}$ and $\kappa_{2\mathit{I}}$	principal curvatures of body I
$\kappa_{1\mathit{II}}$ and $\kappa_{2\mathit{II}}$	principal curvature of body II
$\lambda = (R_i/R_j)^{0.5}$	square root of the ratio of the principal radii of curvature of particles
μ	coefficient of friction
υ_i	Poisson's ratio of particles
ξ_x, ξ_y	longitudinal (in rolling direction) and lateral creepages
σ_s	standard deviation of summit asperity heights
φ	spin creepage
$\phi(z_s)$	Gaussian probability density function
$\phi^*(z_s{}^*)$	standardised summit asperity height distribution whose standard deviation is equal to one
ω	angle between eigenvectors of Hessian Matrix
$\mathbf{\Omega_i}$	angular velocity vector of particle i

1. Introduction

Contact mechanics is of fundamental importance for various problems in both basic and applied research. It was formerly established for comprehending the interaction between relatively large elements, assuming they are continuous and of homogenous properties, e.g., rail-wheel contact or stress distribution in building foundations. Subsequently, it has been used in the simulation of granular particle systems in various engineering fields by the Discrete Element Method (DEM) [1], as reviewed in several papers [2–5]. More recently, contact mechanics is also receiving much attention in emerging fields such as biology and medicine research [6], in which the considered nanoparticles [7] and virus particles [8] are different from granular particles with stronger adhesion, larger surface areas and more complicated shapes. With the extension of DEM to these particle systems [9], accurately modelling the interaction as well as the deformation of the contacting particles is

critical. However, due to the high computational cost of DEM simulation, simplified contact force models for non-spherical shape particles are widely used in DEM studies. Several recent studies demonstrate that these simplified contact force models can bring errors in predicting the contact force and contact area [10,11]. Therefore, more accurate force models should be considered in DEM for simulating particles in these emerging areas.

1.1. Commonly used numerical methods for contact mechanics

For DEM, the contact force calculation should consider both normal and tangential forces, including friction [12], and in both static and dynamic systems [13]. These contact force models are often related to transdisciplinary problems and have been numerically studied by different models, such as the Finite Element Method (FEM), Boundary Element Method (BEM) and Molecular Dynamics (MD) [14–16]. Traditionally, the development of numerical analysis methods in FEM and BEM are the major contributor to the development of contact mechanics [1], which are discussed in this paper. Comparatively, FEM is applicable for problems experiencing small to large deformations in the elastic and inelastic regimes, and BEM is typically applicable for problems with a huge domain scale in which the discretisation of the whole domain is computationally inefficient, and the only boundary needs to be discretised.

With the proliferation of computer technology, both FEM and BEM have been widely employed in the modelling of contact between complex structures. The application of discrete calculation methods is ubiquitous [17]. In FEM, the discretised Hertzian normal contact is modelled. Various contact configurations are defined as *point-to-point*, *point-to-surface*, and *surface-to-surface* to solve contact problems. Furthermore, three-dimensional dynamical contact problems with friction can be solved using spatial point contact models for each discretised contact [17]. The solution algorithm for such contact problems includes the *Penalty method*, the *Lagrangian Multiplier method*, or the combination of both methods, called the *Augmented Lagrangian Method* [1,18]. These methods can be used not only for static problems but also for dynamic loading regimes.

In BEM, the solutions to mechanics problems are approximated by using the boundary integral equations. This technique was first used by Dominguez and Brebbia [19]. The main benefit of BEM is that only the boundary needs to be discretised and the rest of the domain does not need to be discretised regardless of its size if the body force is neglected. BEM was first used by Anderson for solving contact problems [20] and then it was followed by other researchers [21–23]. As the nature of the contact mechanics is that the most of the interesting solutions (e.g., contact pressure, contact area, surface displacement, etc.) are on the contact interface or the boundary, the boundary integral equation has been commonly used by researchers [24,25], in which the domain has been assumed as a half-space or a half-plane. In recent years, the original BEM is attributed with different names, such as finite surface element model [26], conventional deformation matrix method [27], moving grid method [27], etc.

Despite the massive development in FEM and BEM, the analytical solution of contact force is still needed in the Discrete Element Method (DEM). DEM was established by Cundall and Strack [28]. Now it has been widely used for simulating particulate systems in which a large number of discrete, semi-rigid spherical or non-spherical particles come into contact. In DEM, the interaction between particles is calculated using simplified models and hence it is more computationally efficient. However, the well-suited contact force model is a vital component of DEM. In order to develop an analytical formula for contact force, the underlying assumptions of continuum mechanics need to be considered with the so-called elastic half-space hypothesis, as the particles in contact are assumed to be adequately large compared to the contact area in most cases. The deformation of the half-space due to a single-point normal contact force was calculated by Boussinesq [25,29]. For two arbitrary-shaped particles in contact, using the half-space hypothesis for both particles and disregarding friction within the contact interface, the Hertzian classical theory has been established, assuming that the radius of the contact area is much smaller than the radius of the circumscribed sphere of each body [30]. Cattaneo [31] and Mindlin [32] further developed the tangential force-displacement relationship for the Hertzian contact and they employed the assumption of the elastic half-space for the calculation of the force-displacement.

In DEM, once a pair of particles are brought into contact, the contact force is calculated in two steps: (1) geometric calculation and (2) force calculation. The former step is normally called contact detection, which is to calculate the geometric features of the overlap between the two particles, including contact point, contact normal direction, penetration depth or contact volume. The latter step is to determine the resulting contact force based on the contact geometric features. In FEM or BEM, the contact force is modelled based on the contact traction distribution between two contacting elements [32–34], which is dependent on several factors such as shape, surface geometry, material properties, and movement states of particles [35]. However, in order to calculate interactions between many particles in DEM simulation, simplified force models are used without considering the contract traction distribution in detail. These simplified force models were more rigorously established for spherical particles [36–39] but ad-hoc extended to non-spherical particles.

The previous studies on the contact force between non-spherical particles have mainly focused on contact detection algorithms, and less attention has been paid to accurately modelling contact force based on the contact geometric parameters. In fact, for non-spherical contact, in addition to overlap magnitude, the surface curvature plays a key role as well [10]. Therefore, when the accurate prediction of contact forces between non-spherical particles is crucial, more accurate contact force models, which are also more complicated than currently used, could be considered in DEM. The main objective of this paper is to review this kind of models established in contact mechanics, which is to fill the current research gap in step (2) mentioned at the beginning of the previous paragraph. Hereafter, we refer to the models that calculate the contact force based on the overlap geometry as "contact force models", which do not include the overlap calculation part.

1.2. Factors considered in the contact force models

In addition to the overlap geometry, the current contact force models used in DEM normally also consider other facets [6], including: (1) constitutive behaviour of material (i.e. homogeneous/inhomogeneous, elastic/inelastic/viscoelastic, etc), (2) the applied load status (i.e. normal or tangential contact), and (3) the friction and adhesion condition (i.e. frictionless, rough, surface asperity, etc.).

One factor that has not received much attention yet is surface asperity. The effect of the surface feature of particles on the contact force is widely considered in contact mechanics but rarely implemented in DEM. According to the classical Hertzian theory, the shape of the contact patch for two arbitrary-shaped elastic particles in contact is usually elliptical [25]. The Hertzian formulas are solely for the macro-level contact of two particles with ideally curved smooth surfaces. The inclusion of surface roughness in a contact force model is a tedious job due to extreme randomness in the distribution of surface asperities. Substantial research has been undertaken to propose contact models to make accurate predictions. However, it is an insurmountable barrier to measure the real area of the contact with precision to verify the proposed models [40–42]. The contact models for rough surfaces can be categorised in different ways as deterministic models [43–46], the hardness model [47], statistical models [48–51], stacked multi-scale models [52,53], truncation models [54–56], and diffusion models [57,58], but they have rarely implemented in DEM simulations. Recently, Feng et al. [59,60] developed a stochastic DEM framework to predict normal interaction law based on the Greenwood and Williamson

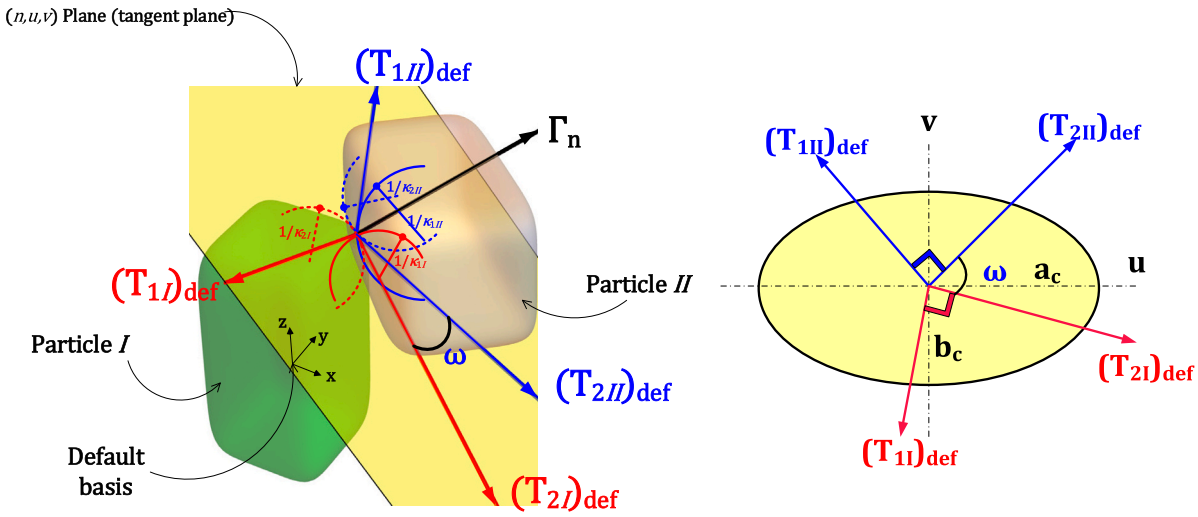

Fig. 1. (a) Definition of the principal curvature and principal direction, courtesy of the Elsevier Journal of Computer Methods in Applied Mechanics and Engineering [10]; (b) contact ellipse in tangent plane.

(GW) model [48], in which a rough surface is assumed to be a compound of asperities whose geometrical features are obtained from a given statistical distribution, and then Hertzian contact law is applied to each spot to obtain overall contact pressure distribution for spherical contact.

Similarly, the adhesion that occurred in the contact has been reasonably implemented in DEM for smooth surfaces. The contact surfaces not only develop repulsive tractions once they are in close proximity, but there is also an attraction acting on the surfaces when they are out of contact. This phenomenon is justified by the inherent characteristics of atoms of the interacted surfaces due to their surface potentials [61]. It is well realised that the nearby contact surfaces will initially be attracted to each other until approaching to the critical distance in which the atoms on one surface tend to repel those on the opposing surface. This trend will cause a bigger contact area compared to the condition where the sole repulsive tractions are considered. In DEM, the surface attraction modelling is vital for small particles in contact when atomic and molecular forces are important [62]. The Johnson, Kendall, Roberts (JKR) [61] and Derjaguin, Muller, and Toporov (DMT) are two well-known models that have incorporated adhesive contacts applicable for soft and hard materials, respectively.

The JKR theory was extended to the general Hertzian theory by Johnson and Greenwood [63] to incorporate elliptical contact areas. The shape of the elliptical contact area was demonstrated to vary in proportion to the applied load. This observation is in contradiction with the classical Hertz theory, assuming a constant rate of ellipse's growth with the increase of the load. Numerical and experimental studies were undertaken to validate elliptical JKR theory. Wu [64] proposed a numerical method for solving the elliptical adhesive contact and the results were compared with the approximate analytical elliptical JKR solution. Sumer et al. [65] investigated the elliptical adhesive contact stress and area using image processing laboratory tests under different loading conditions. Zini et al. [66] extended the double Hertz contact model [67] for predicting adhesive elliptical contact. In particular, the statistical roughness geometry for elliptical contact was investigated by Korayem et al. [7] and appropriate analytical relations based on Hertzian and JKR theory were proposed to solve integral equations.

The damping mechanism has already been implemented in the early DEM models while the treatment is relatively simple compared to contact mechanics. In contact mechanics, surface asperity or roughness may result in excessively small contact areas and relatively high pressure and stress concentration and therefore, local failure or yielding may occur. Hence, plastic deformations must be considered along with elastic deformations once contact force models are taken into account. Classical contact mechanics were extended to incorporate elastic-plastic material behaviour in the prediction of interaction forces [68–72]. An in-depth review of elastic-plastic contact mechanics can be found in [73]. The hypothesis of elastic contact deformation is mostly unrealistic for the flow of granular materials as the coefficient of restitution at impact is generally less than one as a result of plastic deformation occurrence near the contact point [74]. Hence, energy dissipation due to plastic deformation is of particular importance and must be simulated.

Generally, the energy dissipation over particle collision depends on the history of impact and therefore needs to be properly considered in the time integration in DEM. Apart from elastoplasticity techniques, inelastic behaviours are also employed to incorporate energy dissipation in deriving contact laws. The energy dissipation mechanism is employed using viscoelasticity theory to compute the coefficients of restitution for the normal and tangential directions of colliding particles as functions of impact velocity [75].

From the irregular-shaped particles perspective, it is a cumbersome procedure to establish analytical contact interaction principles for particles with sharp corners such as polygon or polyhedron. One common approach to resolve corner singularity is to fictitiously flatten corners by adjusting continuous curves similar to those proposed by Krishnasamy [76] and Houlsby [77]. Alternatively, energy-conservation principle was introduced by Feng et al. [78,79] to resolve contact problems, arisen out of non-smooth particles.

1.3. Aim and structure of the paper

For the factors discussed above, most of the previous theoretical studies on linking contact mechanics to DEM contact force models focused on spherical particles. The latest development in the non-spherical particles contributed by contact mechanics is yet to be implemented in DEM. In this paper, we aim to provide a comprehensive and also targeted review to pave the way for improving the accuracy of DEM through screening suitable candidates of contact force models from contact mechanics, as well as customising and combining them for different situations.

This paper is rationally organised on various aspects of contact force models for non-spherical particles, including (1) type of loading (i.e. normal or tangential) (2) classical Hertzian contact models for non-adhesive particles and Johnson-Kendall-Roberts (JKR) for adhesive particles (3) contact mechanics of particles with rough surfaces (4)

contact mechanics of dissipative contact models (i.e. viscoelastic particles and elastic-plastic/fully plastic regimes), (5) energy-conserving contact models, (6) the extension of Cattaneo-Mindlin-Deresiewicz (CMD) theory for tangential contact forces of non-spherical particles. The main objective of this paper is to review mechanics-based contact force models available for non-spherical bodies in touch, irrespective of how contact detection is performed.

2. Normal contact force models between non-spherical particles

2.1. Hertz theory: Smooth and non-adhesive elliptical contact

In order to compute the normal contact force between non-spherical particles, the contact parameters, such as normal contact overlap and contact radius, are required to be well defined. Fig. 1 shows the schematic of two non-spherical particles *I* and *II* in contact, with the normal contact force, $\mathbf{F}_n$, and the contact area, A_n, to be predicted. According to Hertz theory, the contact initiates at a single point or along a line [25] and then progresses to a finite area (the contact area), which is small compared to the dimensions of the two particles. The following assumptions are used to develop a normal contact force model according to Hertz theory [25], (1) the contact area of two arbitrary-shaped particles in normal contact is, in general, elliptical, (2) each particle can be envisaged as an elastic half-space loaded over the small elliptical region, (3) the significant dimensions of the contact area must be small compared to both dimensions of each body and the relative radii of curvature of the surfaces, and (4) the surfaces of the two particles are assumed to be frictionless and only normal forces are transmitted between them. The normal contact force and contact area can then be given as:

$$\mathbf{F}_n = \frac{4}{3}\widehat{E}_c \widehat{R}_c^{1/2}\delta_n^{3/2}\boldsymbol{\gamma}\mathbf{n} \tag{1}$$

$$A_n = \pi \widehat{R}_c \delta_n \beta \tag{2}$$

where $\widehat{E}_c = \left(\sum_{i=1}^{2}\left(\frac{1-v_i^2}{E_i}\right)\right)^{-1}$.

The above equation is developed according to non-adhesive contact of elastic particles as well as the topographically smooth surfaces of each particle on both micro and macro scales based on Hertz theory. From a micro-scale perspective, it neglects surface irregularities being responsible for highly local variations in contact pressure. From a macro-scale perspective, it assumes the contact surface is continuous up to the second derivative [25].

It is worth noting that the above equations were derived in contact mechanics by applying the external force while solving the overlap. However, in DEM, contact overlap is first determined and then the contact force is calculated based on the overlap. Therefore, in order to implement the above-mentioned formulations in DEM, contact detection algorithms need to be employed to determine the contact parameters, including contact point, contact magnitude and contact normal.

Two popular contact detection algorithms for appropriate prediction of contact overlap and then interaction force are *Geometric Potential* [80–82] and *Common Normal* [62,80,82–84] algorithms. Our previous studies showed the *common normal* algorithm is often more accurate than the *geometric potential* method [11,84]. As previously discussed, here we assume these parameters have been calculated and focus on how to more accurately calculate the contact force based on these parameters.

For particles being mathematically represented by a continuous function with continuous first and second derivatives, the parameter $\widehat{R}_c$ in Eq. (1) can be calculated by finding principal curvatures and direction at the contact point on the surface of two bodies [25,85], given as,

$$\frac{1}{R_i} = 0.5\Big\{(\kappa_{1I}+\kappa_{2I}+\kappa_{1II}+\kappa_{2II}) - \big[(\kappa_{1I}-\kappa_{2I})^2 + (\kappa_{1II}-\kappa_{2II})^2 + 2(\kappa_{1I}-\kappa_{2I})(\kappa_{1II}-\kappa_{2II})cos2\omega\big]^{0.5}\Big\}$$

$$\frac{1}{R_j} = 0.5\Big\{(\kappa_{1I}+\kappa_{2I}+\kappa_{1II}+\kappa_{2II}) + \big[(\kappa_{1I}-\kappa_{2I})^2 + (\kappa_{1II}-\kappa_{2II})^2 + 2(\kappa_{1I}-\kappa_{2I})(\kappa_{1II}-\kappa_{2II})cos2\omega\big]^{0.5}\Big\}$$

$$\widehat{R}_c = \frac{R_i R_j}{R_i + R_j} \tag{5}$$

(κ_{1I}, κ_{2I}) and (κ_{1II} and κ_{2II}) are principal curvatures of body *I* and *II* which may be found as eigenvalues of Hessian Matrix, $\mathbf{H}_{uv}^{n}$, given as

$$\mathbf{H}_{uv}^{n} = \begin{bmatrix} \frac{\partial^2 \Gamma}{\partial u^2} & \frac{\partial^2 \Gamma}{\partial u \partial v} \\ \frac{\partial^2 \Gamma}{\partial v \partial u} & \frac{\partial^2 \Gamma}{\partial v^2} \end{bmatrix} \tag{6}$$

In our recent study, it is shown that to accurately calculate the contact force, the principal curvatures and directions need to be rigorously calculated using the following expressions [10]:

$$\kappa_1 = K_M + \sqrt{|K_M{}^2 - K_G|}\ \kappa_2 = K_M - \sqrt{|K_M{}^2 - K_G|} \tag{7}$$

$$\omega = \frac{(\mathbf{T_{1I}})_{\mathbf{def}}\cdot(\mathbf{T_{1II}})_{\mathbf{def}}}{\left\|(\mathbf{T_{1I}})_{\mathbf{def}}\right\|\left\|(\mathbf{T_{1II}})_{\mathbf{def}}\right\|} \tag{8}$$

$(\mathbf{T_{1I}})_{\mathbf{def}}$ and $(\mathbf{T_{1II}})_{\mathbf{def}}$ are defined as follows [10]:

$$(\mathbf{T_1})_{\mathbf{def}} = \frac{1}{\sqrt{\left(\frac{\partial^2\Gamma}{\partial u \partial v}\right)^2 + \left(\kappa_1\Gamma\backslash - \frac{\partial^2\Gamma}{\partial u^2}\right)^2}} \begin{pmatrix} \left(\kappa_1\Gamma\backslash - \frac{\partial^2\Gamma}{\partial u^2}\right).\prime_x + \frac{\partial^2\Gamma}{\partial u \partial v}\prime\prime_x \\ \left(\kappa_1\Gamma\backslash - \frac{\partial^2\Gamma}{\partial u^2}\right).\prime_y + \frac{\partial^2\Gamma}{\partial u \partial v}\prime\prime_y \\ \left(\kappa_1\Gamma\backslash - \frac{\partial^2\Gamma}{\partial u^2}\right).\prime_z + \frac{\partial^2\Gamma}{\partial u \partial v}\prime\prime_z \end{pmatrix} \tag{9}$$

$$(\mathbf{T_2})_{\mathbf{def}} = \frac{1}{\sqrt{\left(\frac{\partial^2\Gamma}{\partial u \partial v}\right)^2 + \left(\kappa_2\Gamma\backslash - \frac{\partial^2\Gamma}{\partial v^2}\right)^2}} \begin{pmatrix} \left(\kappa_2\Gamma\backslash - \frac{\partial^2\Gamma}{\partial v^2}\right).\prime_x + \frac{\partial^2\Gamma}{\partial u \partial v}\prime\prime_x \\ \left(\kappa_2\Gamma\backslash - \frac{\partial^2\Gamma}{\partial v^2}\right).\prime_y + \frac{\partial^2\Gamma}{\partial u \partial v}\prime\prime_y \\ \left(\kappa_2\Gamma\backslash - \frac{\partial^2\Gamma}{\partial v^2}\right).\prime_z + \frac{\partial^2\Gamma}{\partial u \partial v}\prime\prime_z \end{pmatrix} \tag{10}$$

where $\mathbf{u}^t = (\prime_x, \prime_y, \prime_z)^t$, $\mathbf{v}^t = (\prime\prime_x, \prime\prime_y, \prime\prime_z)^t$ are arbitrary orthogonal unit vectors in tangent contact plane.

Details of principal curvatures and principal directions for two arbitrary particles in contact is shown in Fig. 1.

Based on such accurate contact geometry model, the correction factors γ and β in eq. (1) and (2) can be calculated as

$$\gamma = \frac{\pi\sqrt{2}(\mathbb{E}(e^2))^{0.5}}{2(\mathbb{K}(e^2))^{1.5}(1-e^2)^{0.5}} \tag{11}$$

$$\beta = \frac{2\mathbb{E}(e^2)}{\mathbb{K}(e^2)(1-e^2)^{0.5}} \tag{12}$$

where $\mathbb{K}(e^2) = \int_0^{\pi/2}(1-e^2 sin^2\varphi)^{-0.5}d\varphi$, $\mathbb{E}(e^2) = \int_0^{\pi/2}(1-e^2 sin^2\varphi)^{0.5}d\varphi$. Contact eccentricity in the eqs. (11) and (12) can be calculated as a solution of the following functional equation

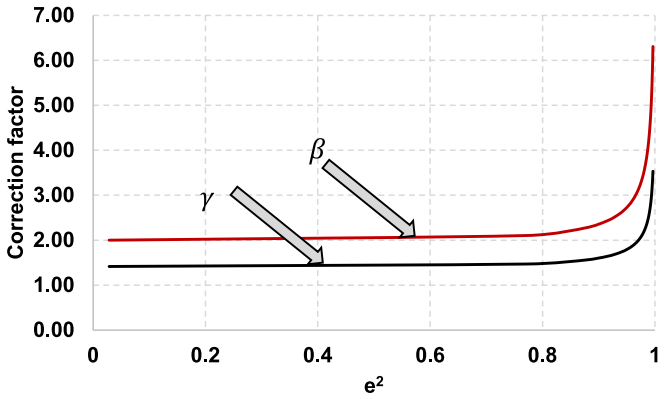

Fig. 2. Variation of correction factors for calculating contact force and overlap area with respect to contact eccentricity.

$$e^2 = 1 - \frac{\frac{R_i}{R_j}\mathbb{E}(e^2)}{\left(\frac{R_i}{R_j}+1\right)\mathbb{K}(e^2) - \mathbb{E}(e^2)} \tag{13}$$

The following simplified formula can be used to calculate contact elliptical eccentricity.

$$e^2 = 1 - \left\{ -0.177 + \left(0.5\left(\frac{R_i}{R_j}\right)^{-1} ln\left[16\left(\frac{R_i}{R_j}\right)^{-1}\right]\right)^{0.5} + 0.16 ln\left[\left(\frac{R_i}{R_j}\right)\right]\right\}^{-2} \tag{14}$$

In Fig. 2, the variation of correction factors for contact normal force and area with respect to contact eccentricity is plotted. Detailed numerical examples demonstrating that the accurate geometrical force model is better than those simplified models when compared to FEM simulations can be found in our previous study [33] and some numerical examples will be shown later.

As discussed earlier, Hertz's theory postulates semi-infinite bodies in contact, it is imperative to specify the greatest ratio of semi-major axis of contact ellipse to smallest radius of curvature to which the theory could be applied. Fessler and Ollerton [86] conducted experiments in an attempt to determine the range of applicability. They concluded that the differences between theoretical and experimental values are small when the ratio of the semi-major axis of the contact ellipse to the smallest radius of curvature of the contacting particles is smaller than 0.5.

The abovementioned contact force model can be directly employed for a wide variety of non-spherical particle shapes having continuous surface function representation and convex surface, such as super-quadrics given by,

$$\Gamma(x,y,z) = \left(\left(\frac{x}{a}\right)^{2/\eta_2} + \left(\frac{y}{b}\right)^{2/\eta_2} \right)^{\eta_2/\eta_1} + \left(\frac{z}{c}\right)^{2/\eta_1} - 1 = 0 \tag{15}$$

in which η_1 and η_2 control the squareness of the particle in the $y-z$, $x-z$, and $x-y$ planes, respectively. The ellipsoid particles are also included and can be obtained by setting $\eta_1 = \eta_2 = 1$.

For more complex shapes such as polygonal or polyhedral particles, the method proposed by Houlsby [77] can be employed to substitute the original particle with the form having rounded corners, edges, and faces, called "potential particle". Houlsby [77] proposed particles composed of planes with the corresponding potential function of the form,

$$\Gamma(x,y,z) = (1-k)\left\{ \sum_{i=1}^{n} \langle a_i x + b_i y + c_i z + d_i \rangle^2 - r^2 \right\} + k\left(x^2 + y^2 + z^2 - R^2\right) = 0 \tag{16}$$

in which $\langle\rangle$ is the Macaulay bracket.

The above equations provide an accurate geometrical model to calculate contact force [10]. To demonstrate the accuracy and efficiency of the accurate geometrical force model against simplified equations in literature, the simplified model proposed in [87] is used for comparison. The general form of simplified force model is similar to eq. (1), except that the correction factor (γ) is always 1 and R_i and R_j are calculated as follows instead of eqs. (3) and (4):

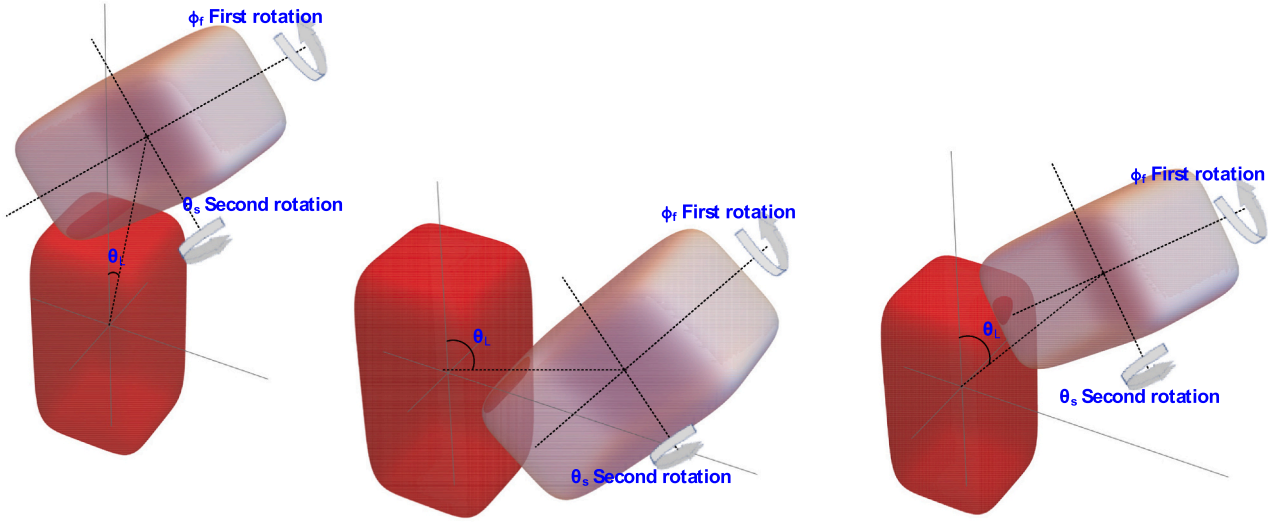

(a) Case1 (b) Case2 (c) Case3

Fig. 3. Non-spherical particles in touch (a) $\theta_L = 10^\circ$; $\varphi_f = 80^\circ$; $\theta_s = 50^\circ$; (b) $\theta_L = 70^\circ$, $\varphi_f = 90^\circ$, $\theta_s = 40^\circ$; (c) $\theta_L = 40^\circ$, $\varphi_f = 70^\circ$, $\theta_s = 50^\circ$.

Table 1
Comparison of the simplified contact force model and the accurate contact force model.

		$\mathbf{F}_n/\left(\frac{4}{3}\widehat{E}_c R_{vol}^{1/2}\delta_n^{3/2}\right)$	D_v (%)	Computation time (Sec)
Accurate Geometrical Model	Case1	1.5911	7	0.123
	Case2	1.5923	2	0.049
	Case3	0.5345	2	0.12
Simplified Model	Case1	2.2361	51	0.120
	Case2	2.2361	37	0.048
	Case3	2.2361	310	0.118
Finite element	Case1	1.4855		
	Case2	1.6306	–	–
	Case3	0.5460		

$$\frac{1}{R_i} = \sqrt{K_{G,I}} \tag{17}$$

$$\frac{1}{R_j} = \sqrt{K_{G,II}} \tag{18}$$

where $K_{G,\ I} = \kappa_{1I}\kappa_{2I}$ and $K_{G,\ II} = \kappa_{1II}\kappa_{2II}$ are, respectively, Gaussian curvature of particle I and II, as discussed in [87]. One issue for the simplified model is that the radii in eqs. (17) and (18) may become infinity when the Gaussian curvature is zero. The Gaussian curvature becomes zero if any of the principal curvature is zero. To overcome this issue, here the radii of curvature in eqs. (17) and (18) are limited to $10R_{vol}$, where R_{vol} is the radius of the volume equivalent sphere of the particle. The accurate geometrical force model does not have this issue.

To conduct quantitative comparison, two non-spherical particles with the governing skin eq. (15) ($\eta_1 = \eta_2 = 1/3$, $a/b = c/2b = 1$) are chosen with the Eulerian orientations shown in Fig. 3 The setup is similar to our previous work and the details can be found in ref. [10]. In Table 1., normalised normal contact forces obtained from simplified model and the accurate geometrical model are compared to the FEM simulation (details of FEM the model can be found in ref. [10]). In addition, the computation times using the two models are also reported. As seen, the accurate geometrical model shows substantial improvement in accuracy compared to the simplified model, because of the accurate prediction of the radii of curvatures and the correction factor (γ). There is generally a minor increase in the computation time by about 2%–3%. It is worth noting that the calculations are conducted by using the software, Wolfram Mathematica [88]. Implementing the model in other computer languages may cause a higher increase in the computation time. However, the increase should be reasonable and worthwhile for the significant improvement in accuracy. Moreover, the errors of the curvature will also affect the contact force model with surface properties considered, as will be shown in the following sections.

2.2. Johnson-Kendal-Roberts (JKR) model: Smooth and adhesive elliptical contact

It is well recognised that to separate two particles in contact, mechanical work is required to overcome the adhesive forces [61]. This energy can be introduced as a free surface energy and be measured according to the theory of adhesion of elastic contacts, as developed by Johnson et al. [61] in the JKR theory. The JKR theory was originally implemented to circular contacts and then extended to general Hertzian contacts, where the contact areas would be elliptical regardless of surface forces. Due to adhesion forces developed by surface energy, the eccentricity of a contact ellipse is no longer predicted by Hertz theory, and is dependent on the load [63].

In the JKR theory for elliptical contacts, which can be used for contact between non-spherical particles, the work of adhesion due to contact energy release rate is assumed to be an ellipse with the semi-major of a_c and the semi-minor axis of b_c. The primary hypothesis of this model is the equal stress intensity factors along the major and minor axes at the edges of the contact area. The Johnson greenwood (JG) analytical approximation presents the solution of dimensionless normal load ($\overline{F_n}$), indentation depth ($\overline{\delta_n}$), and contact area ($\overline{A_n}$) [63].

$$\overline{F_n} = \frac{F_n}{3\pi\widehat{R}_{c1}W_{ad}} = \frac{8}{3\pi}\frac{g\left(1-g^{1/2}\right)^2}{\left(\Pi_2 g^2-\Pi_1\right)^2}\left[\frac{\Pi_1-\Pi_2 g^{5/2}}{1-g^{1/2}} - \frac{1}{3}\left(\Pi_2 g^2+\Pi_1\right)\right] \tag{19}$$

$$\overline{\delta_n} = \delta_n\left(\frac{4\widehat{E}_c}{9\pi W_{ad}\widehat{R}_{c1}^{0.5}}\right)^{2/3} = \left(\frac{2^{7/2}}{9\pi^2}\right)^{2/3}\left[\frac{g\left(1-g^{1/2}\right)^2}{\left(\Pi_2 g^2-\Pi_1\right)^2}\right]^{2/3}\left[2\mathbb{K}\left(e^2\right)\frac{\Pi_1-\Pi_2 g^{5/2}}{1-g^{1/2}} - \Pi_1\mathbb{B}\left(e^2\right) - g^2\Pi_2\mathbb{D}\left(e^2\right)\right] \tag{20}$$

$$\overline{A_n} = A_n\left(\frac{4\widehat{E}_c}{9\pi^{5/2}W_{ad}\widehat{R}_{c1}^2}\right)^{2/3} = \left(\frac{4\sqrt{2}}{3\pi}\frac{g^{5/4}\left(1-g^{1/2}\right)}{\Pi_2 g^2-\Pi_1}\right)^{4/3} \tag{21}$$

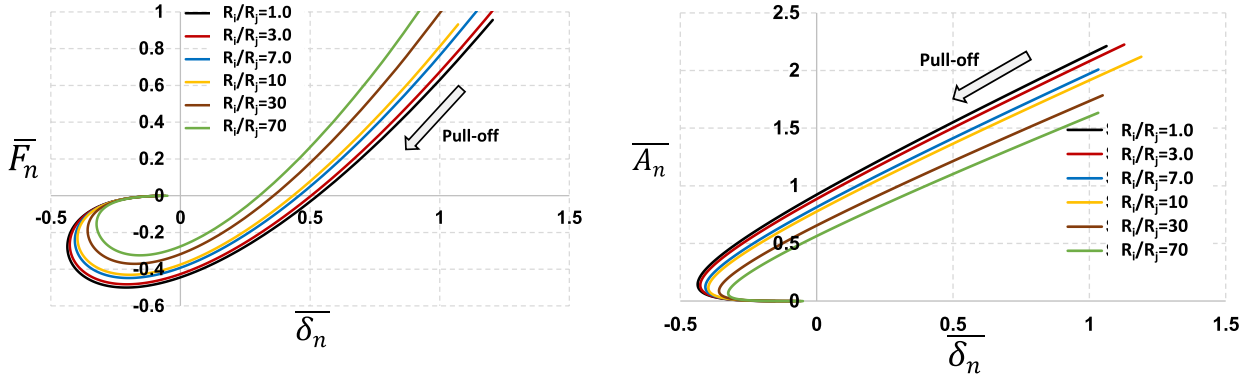

(a) **(b)**

Fig. 4. (a) Dimensionless force-indentation from pull-off simulation for elliptical contact; (b) dimensionless area-indentation from pull-off simulation for elliptical contact.

Table 2
Elliptical contact force calculation for adhesive particles in touch.

	$\mathbf{F}_n/\left(\frac{4}{3}\widehat{E}_c R_{vol}^{1/2}\delta_n^{3/2}\right)$	$\widehat{R}_c/R_{vol}$	γ_{JG}	Computation time (Sec)
Case1	1.5872	1.507	1.292	0.124
Case2	1.5884	1.512	1.292	0.050
Case3	0.5334	0.283	1.003	0.122

where $g = b_c/a_c$ is the axis ratio which is related to the eccentricity of the contact ellipse by $e^2 = 1 - g^2$, $\widehat{R}_{c1} = \sqrt{R_i R_j}$, $\lambda = (R_i/R_j)^{1/2}$, λ must be less than unity, and W_{ad} is the work of surface adhesion. Π_1 and Π_2 are dimensionless parameters accounting the effect of adhesion energy as

$$\Pi_1 = \frac{\lambda + \lambda^{-1} - \mathbb{B}(e^2)\Pi_2}{\mathbb{D}(e^2)} \tag{22}$$

$$\Pi_2 = \frac{\left(\lambda^2+1\right)\mathbb{C}(e^2) + \mathbb{D}(e^2)}{\lambda\left[\left(\mathbb{D}(e^2)+\mathbb{C}(e^2)\right)\left(\mathbb{B}(e^2)+g^2\mathbb{C}(e^2)\right) - g^2\left(\mathbb{C}(e^2)\right)^2\right]} \tag{23}$$

$\mathbb{B}(e^2)$, $\mathbb{C}(e^2)$, and $\mathbb{D}(e^2)$ are complete elliptic integrals given by:

$$\mathbb{D}\left(e^2\right) = \frac{\mathbb{K}(e^2) - \mathbb{E}(e^2)}{e^2} \tag{24}$$

$$\mathbb{B}\left(e^2\right) = \mathbb{K}\left(e^2\right) - \mathbb{D}\left(e^2\right) \tag{25}$$

$$\mathbb{C}\left(e^2\right) = \frac{\mathbb{D}(e^2) - \mathbb{B}(e^2)}{e^2} \tag{26}$$

The maximum tensile force that the contact can resist is the imperative characteristic of an adhesive contact. The dimensionless force-indentation and area-indentation curves for pull-off simulation and different values of R_j/R_i are plotted in Fig. 4, which shows that the curvature calculation will further affect the contact force model for the adhesive particles.

The normal contact force and contact area can still be calculated using eqs. (1) and (2), except that correction factors γ and β need to be, respectively, replaced by γ_{JG} and β_{JG} given below, and $\widehat{R}_c$ in eq. (5) also needs to be replaced by $\widehat{R}_{c1} = \sqrt{R_i R_j}$. Here we recommend R_i and R_j to be calculated according to Eqs. (3) and (4), as these variables may have other definitions in the literature.

$$\gamma_{JG} = \frac{3\pi\sqrt{2}}{2}\frac{\frac{\Pi_1 - \Pi_2 g^{5/2}}{1-g^{1/2}} - \frac{1}{3}\left(\Pi_2 g^2 + \Pi_1\right)}{\left(2\mathbb{K}(e^2)\frac{\Pi_1 - \Pi_2 g^{5/2}}{1-g^{1/2}} - \Pi_1\mathbb{B}(e^2) - g^2\Pi_2\mathbb{D}(e^2)\right)^{3/2}} \tag{27}$$

$$\beta_{JG} = \frac{2g}{\mathbb{K}(e^2)\frac{\Pi_1 - \Pi_2 g^{5/2}}{1-g^{1/2}} - \Pi_1\mathbb{B}(e^2) - g^2\Pi_2\mathbb{D}(e^2)} \tag{28}$$

Using the above equations, we calculate the three contact cases given in Fig. 3. with adhesion considered, and the results are listed in Table 2. It can be seen that the contact geometrical parameters change with the adhesion considered, while the computation time is similar to the previous non-adhesion model.

2.3. Non-smooth (rough) particles

In reality, the surface of particles is not smooth, and the surface roughness will cause a substantially small contact area compared to the nominal area [48,59], which will affect the contact force. Once such surfaces are pressed against each other, the contact initiation will occur at discrete micro protrusions called asperity tips. The contact force is normally developed at a limited number of asperities and then spreads over a larger area as the normal force increases. Surface asperities have a substantial influence on the real contact area and contact resistance. The most prominent approach to consider rough surfaces is the Greenwood and Williamson (GW) model [48], in which a statistical height distribution is assigned to a set of compound asperities to define a rough surface and then the resultant contact force is defined by the summation of local Hertzian contact force being developed at each asperity. The assumptions behind the GW rough contact model are (1) the height distribution of surface asperities (the distance from the surface) is assumed to be Gaussian normal distribution, (2) the interaction between asperities is neglected, and (3) the material properties of asperities are isotropic and similar to the base particle material. The resultant contact force, F_r, and contact area, A_r, for elliptical contact, are obtained by integrating contact forces and areas, developed at each asperity, given by:

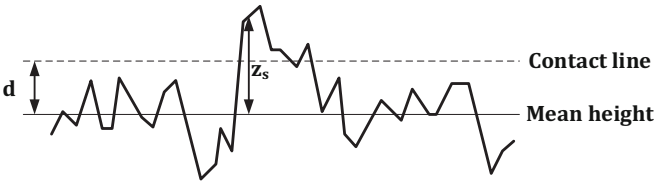

Fig. 5. Schematic view of the contact of the rough surfaces.

$$F_r = NA_n\int_d^\infty f(z_s - d)\phi(z_s)dz_s \tag{29}$$

$$A_r = NA_n\int_d^\infty A(z_s - d)\phi(z_s)dz_s \tag{30}$$

in which z_s and d are shown in Fig. 5, and $\phi(z_s) = \frac{1}{\sqrt{2\pi}\sigma_s}exp\left(-\frac{z_s^2}{2\sigma_s{}^2}\right)$.

Eqs. (29) and (30) can be rewritten for non-dimensional parameter ($z_s^* = \frac{z_s}{\sigma_s}$) as [88]:

$$F_r = \frac{4}{3}NA_n\widehat{E}_c\widehat{R}_c^{1/2}\sigma_s^{3/2}\gamma\int_h^\infty\left(z_s^* - h\right)^{3/2}\phi^*\left(z_s^*\right)dz_s^* \tag{31}$$

$$A_r = \pi NA_n\widehat{R}_c\sigma_s\beta\int_h^\infty\left(z_s^* - h\right)\phi^*\left(z_s^*\right)dz_s^* \tag{32}$$

in which $h = \frac{d}{\sigma_s}$ and $\phi^*\left(z_s^*\right) = \frac{1}{\sqrt{2\pi}}exp\left(-\frac{z_s^{*2}}{2}\right)$. Therefore, the resultant contact force and area for rough contact can be expressed as,

$$F_r = \frac{4}{3}NA_n\widehat{E}_c\widehat{R}_c^{1/2}\sigma_s^{3/2}\gamma^* \tag{33}$$

$$A_r = \pi NA_n\widehat{R}_c\sigma_s\beta^* \tag{34}$$

where $\widehat{R}_c$ should be calculated using Eqs. (3)–(5) for non-spherical particles, and $\gamma^* = \gamma_{GW}{}^*$ and $\beta^* = \beta_{GW}{}^*$ are given as follows [89]:

$$\gamma_{GW}^* = \gamma\frac{1}{4\sqrt{\pi}}exp\left(\frac{-h^2}{4}\right)\sqrt{h}\left[\left(h^2+1\right)\mathscr{K}_{1/4}\left(\frac{h^2}{4}\right) - h^2\mathscr{K}_{3/4}\left(\frac{h^2}{4}\right)\right] \tag{35}$$

$$\beta_{GW}^* = \beta\left(\frac{1}{\sqrt{2\pi}}exp\left(\frac{-h^2}{4}\right) - \frac{1}{2}herf\left(\frac{h}{\sqrt{2}}\right)\right) \tag{36}$$

where $erf(x) = \frac{2}{\sqrt{\pi}}\int_0^x exp\left(-t^2\right)dt$ and $\mathscr{K}_\vartheta(z)$ is the modified Bessel function of the second kind for non-integer ϑ.

The correction factors γ and β in Eqs. (35) and (36) can be obtained from either the Hertzian model or the JKR model based on whether non-adhesive particles or adhesive particles are considered. In Fig. 6, the variation of contact area and contact force correction factors obtained from the GW model with respect to standardised separation for various ratios of R_j/R_i is plotted, which shows that they may vary in a certain range, and hence will still result in much difference in the calculated contact force and contact area. More importantly, the accurate geometrical model can give better prediction with the curvature more precisely calculated.

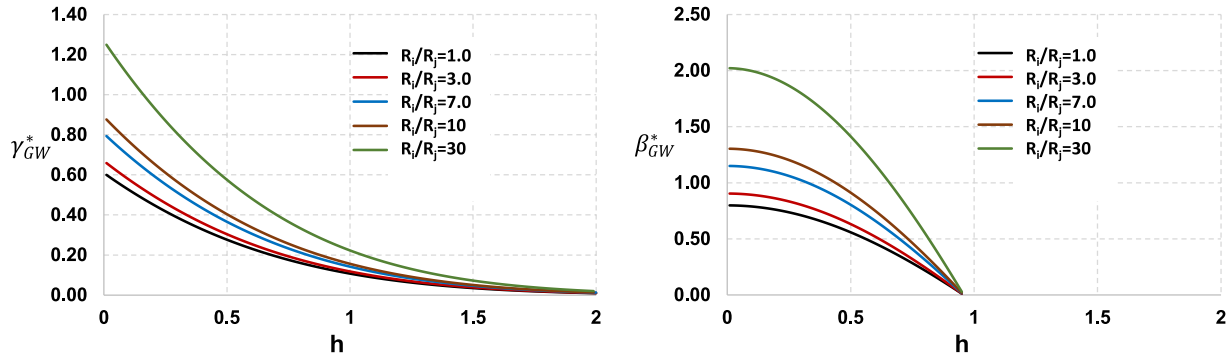

(a) (b)

Fig. 6. Variation of correction factors of GW model with respect to standardised separation: (a) contact force correction factor, (b) contact area correction factor.

Table 3
Elliptical contact force calculation for rough particles in touch.

		$\mathbf{F}_n/\left(\frac{4}{3}NA_n\widehat{E}_cR_{vol}^{1/2}\sigma_s^{3/2}\right)$	$\widehat{R}_c/R_{vol}$	$\gamma_{GW}{}^*$	Computation time (Sec)
Case1	h = 0.01	0.6744	0.222	1.431	0.117
	h = 1.00	0.0183		0.255	
Case2	h = 0.01	0.6749	0.223	1.428	0.045
	h = 1.00	0.1205		0.255	
Case3	h = 0.01	0.2266	0.136	0.614	0.118
	h = 1.00	0.0404		0.110	

In Table 3, the previous three contact cases are calculated with different h by Eq. (35). It can be seen that the roughness has a significant effect on the contact force as well as the contact geometrical parameters, which is worthy of attention in DEM modelling. Interestingly, the computation time is similar to the previous model. It further shows that the calculation of the geometrical parameters such as the curvatures will be most time consuming.

2.4. Normal dissipative force

Aside from conservative elastic forces commonly considered in the collision of granular particles, dissipative forces due to the dissipation of mechanical energy are also important [90,91]. The reason for the formation of these forces is the massive number of microscopic degrees of freedom in particulate systems that partly absorbs translational and rotational internal energies. Therefore, the interparticle force is a compound of elastic and dissipative force components. The aforementioned contact force models are for elastic interaction regimes. Several researchers proposed an extended form of the Hertzian contact force model to accommodate energy dissipation [75,92]. The dissipative forces according to the Hertzian contact model can be calculated using the following expression [90]:

$$\mathbf{F}_{\mathbf{n-dis}} = A\dot{\delta}_n\frac{\partial \mathbf{F_n}}{\partial \delta_n} = 2A\widehat{E}_c\widehat{R}_c^{1/2}\delta_n^{1/2}\dot{\delta}_n\boldsymbol{\gamma}\mathbf{n} \tag{37}$$

The total normal contact force is then calculated by adding elastic Hertzian force to dissipative viscoelastic force as follows:

$$\mathbf{F}_{\mathrm{n-V}} = \widehat{E}_c\widehat{R}_c^{\frac{1}{2}}\delta_n^{\frac{1}{2}}\left(\frac{4}{3}\delta_n + 2A\dot{\delta}_n\right)\boldsymbol{\gamma}\mathbf{n} \tag{38}$$

where $A = 1/3[(3\eta_{2i} - \eta_{1i})^2/(3\eta_{2i} + 2\eta_{1i})][(1 - v_i^2)(1 - 2v_i)/E_iv_i^2]$.

As the adhesive interaction forces between particles lead to supplementary deformation in the bodies in touch in comparison to the classical Hertz theory, in the associated dynamical problems the additional deformation rates are expected and dissipated forces must include another term associated with the adhesive interactions according to the JKR theory. The dissipative adhesive contact force can be given by [90]:

$$\mathbf{F}_{\mathbf{n-dis}} = \left(2A\widehat{E}_c\widehat{R}_c^{1/2}\delta_n^{1/2}\dot{\delta}_n\gamma + \frac{3}{4}B\sqrt{\frac{\pi q}{D}}\widehat{R}_c{}^{3/4}\dot{\delta}_n\delta_n^{-1/4}\right)\mathbf{n} \tag{39}$$

where $D = 3/4\widehat{E}_c$, $B = (3\eta_{2i} - \eta_{1i})E_iv_iq_0/3(1 + v_i)(1 - 2v_i)$, $q_0 = \sqrt{6} -$

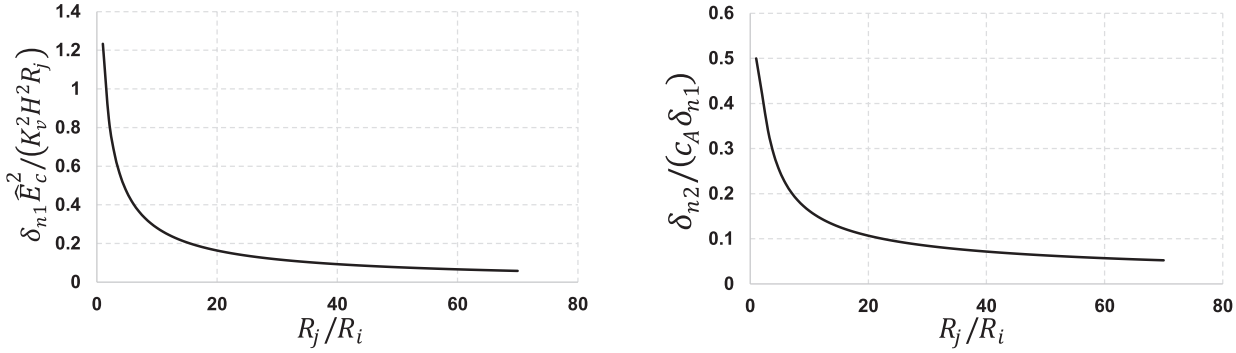

(a) Critical normal overlap (δ_{n1}) (b) onset of fully plastic normal contact overlap (δ_{n2})

Fig. 7. Variation of normal overlaps versus the ratio of radii of curvatures at contact point.

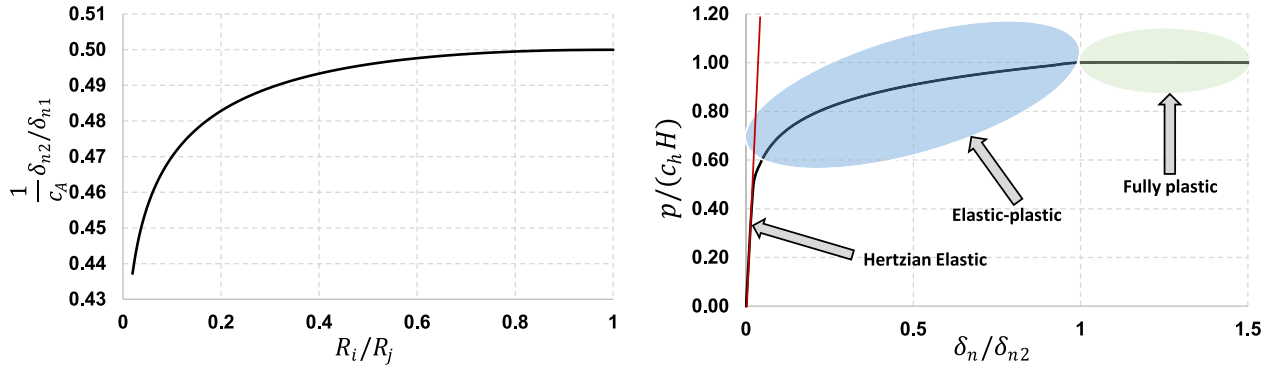

(a) (b)

Fig. 8. Initiation of full plasticity as a function of ellipticity ratio R_i/R_j.

$\sqrt{8/3}$, and ϱ is the work of adhesion. The elastic plus viscoelastic adhesive contact force can be expressed as:

$$\mathbf{F_{n-V}} = \widehat{E}_c \widehat{R}_c^{\frac{1}{2}} \delta_n^{\frac{1}{2}} \left(\frac{4}{3}\delta_n \gamma + 2A\dot{\delta}_n \gamma + \frac{3}{4} B \sqrt{\frac{\pi \varrho}{D}} \widehat{R}_c^{\,1/4} \dot{\delta}_n \delta_n^{-3/4} \right) \mathbf{n} \tag{40}$$

2.5. Elastic-plastic and fully plastic contacts

2.5.1. Smooth elastic-plastic and fully plastic contact

As initial material yielding at the contact area occurs once the maximum contact pressure, p_m, touches the value of $p_m = K_v H$ [68], where K_v is the multiplier. According to eqs. (1) and (2) and maximum contact pressure, the critical normal overlap, δ_{n1}, can read as

$$\delta_{n1} = \frac{\pi^2}{4} \widehat{R}_c \frac{\beta^2}{\gamma^2} \frac{K_v^2 H^2}{\widehat{E}_c^2} = 2\widehat{R}_c \frac{K_v^2 H^2}{\widehat{E}_c^2} \mathbb{E}(e^2) \mathbb{K}(e^2) \tag{41}$$

It was shown that the contact area for the fully plastic regime, A_p, for the elliptical contact situation may be calculated using the following expression [93]:

$$A_p = 2\pi (R_i R_j)^{0.5} \delta_n \tag{42}$$

F_{n-P} is equal to fully plastic contact area multiplied by contact mean pressure as [94]:

$$F_{n-P} = 2\pi \delta_n (R_i R_j)^{0.5} c_h H \tag{43}$$

δ_{n2} can be calculated by conducting mathematical manipulations on eqs. (1), (41), and (43) as

$$\delta_{n2} = c_A \left(\frac{\lambda}{1+\lambda^2} \right) \frac{1}{(1-e^2)^{1/2}} \frac{\mathbb{E}(e^2)}{\mathbb{K}(e^2)} \delta_{n1} \tag{44}$$

The contact load and contact area in the elastic-plastic regime can be expressed by the following formula [94]:

$$F_{n-EP} = A_{n-EP} \left[c_h H - H \left(c_h - \frac{2}{3} K_v \right) \frac{ln\delta_{n2} - ln\delta_n}{ln\delta_{n2} - ln\delta_{n1}} \right] \tag{45}$$

$$A_{n-EP} = \pi \widehat{R}_c \delta_n \beta + \left(2\pi (R_i R_j)^{0.5} \delta_n - \pi \widehat{R}_c \delta_n \beta \right) \left[3 \left(\frac{\delta_n - \delta_{n1}}{\delta_{n2} - \delta_{n1}} \right)^2 - 2 \left(\frac{\delta_n - \delta_{n1}}{\delta_{n2} - \delta_{n1}} \right)^3 \right] \tag{46}$$

Fig. 7 shows the variation of critical normal overlap and fully plastic normal overlap versus the ratio of radii of curvatures at contact point. Furthermore, Fig. 8(a) shows the fully plastic contact initiation as a function of the ellipticity ratio, R_i/R_j, according to eq. (44). Evidently, the curvature values affect this critical parameter. In particular, for the range of R_i/R_j of 0.6 to 1.0, $\delta_{n2}/(c_A\delta_{n1})$ is nearly at the value of 0.5. Generally, the full plastic contact initiation is almost independent of the shape of the contact ellipse [93]. Fig. 8(b) illustrates the non-dimensional mean contact pressure, $p/(c_hH)$, as a function of non-dimensional contact indentation, δ_n/δ_{n2}. This figure covers the contact model from the Hertzian elastic to fully plastic contact regime.

2.5.2. Non-smooth elastic-plastic and fully plastic contact

Once two particles come into contact, surface asperities initially interact with each other to form micro-contact, followed by the plastic deformation development and macro-contact formation. Regarding the load carrying capacity of surface asperities, the contact deformation may exceed the elastic range and show either elastic-plastic or fully plastic behaviour [95,96]. The GW model gives reliable results compared to available isotropic models for rough contact status [97]. Nevertheless, it can be applied to contact where the contacting asperities mostly deform elastically. Chang, Etsion and Bogy (CEB) [68] developed the CEB model in which the effects of plastic deformation at surface asperities are included in the GW model by using volume conservation for plasticity deformed asperities. They introduced a critical interface cut-off (δ_{n1}) for the elastic deformation in which fully plastic deformation is assumed beyond this value. Jeng and Wang [98] proposed an elliptic microcontact model considering the elastic, elastic-plastic and fully plastic deformation, based on the assumptions: (1) the surface roughness is isotropic, (2) all surface spike summits' heights follow the Gaussian distribution, (3) all surface spikes are spherical near their summits and have the same radius of curvature, (4) there are no interactions between surface spikes, (5) during contact progression only the surface spikes deform, and no bulk deformation is taken into account. The contact force model and contact area for regimes of elastic,

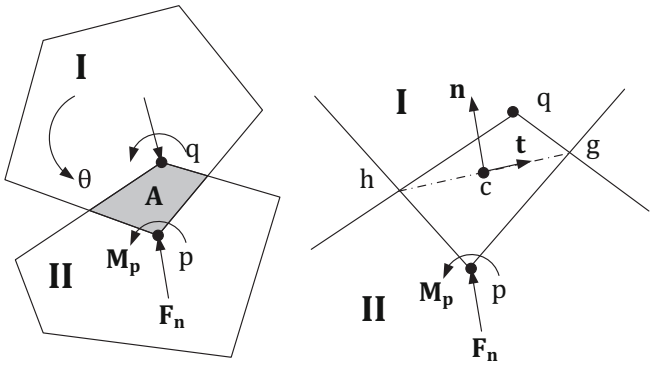

Fig. 9. (a) Contact between two polygons; (b) normal contact model.

elastic-plastic, and fully plastic deformation were proposed by Eqs. (33) and (34) with γ^* and β^* as [98]:

small amount of overlap could occur. For two contacting bodies I and II as shown in Fig. 9, the motion of the system can be fully defined by rotational and translational degrees of freedom of body I provided the body II is fully fixed. The overlap area (A) is enclosed by four points as: penetrating vertices, p and q, as well as intersecting edges at g and h. The middle point of the connecting line between points g and h was assumed to be reference contact point. The pair of normal contact force and bending moment $(\mathbf{F}_n, M_{\mathscr{P}})$ imposed by a fixed body (i.e. body I) to a moving body (i.e. body II) can be expressed by the following formula:

$$\mathbf{F}_n = \|\mathbf{F}_n\|\mathbf{n} = -\left\{W'(A)\left\|\nabla_{\mathbf{x}_p}A\right\|\right\}\left\{\frac{\nabla_{\mathbf{x}_p}A}{\left\|\nabla_{\mathbf{x}_p}A\right\|}\right\} \tag{54}$$

$$M_{\mathscr{P}} = -W'(A)\frac{\partial A(\mathbf{x}_p,\theta)}{\partial\theta} \tag{55}$$

where $W(A)$ is the contact energy potential of overlap area (A), $\mathbf{x}_p = \left\{\mathscr{x}_p, \mathscr{y}_p\right\}$ is the cartesian coordinates of vertex p, $\nabla_{\mathbf{x}_p}A$ is the gradient of A

$$\gamma^* = \gamma\int_h^{h+\delta_{n1}^*}(z_s^*-h)^{3/2}\phi^*(z_s^*)dz_s^* + \frac{3\pi H}{2\widehat{E}_c}\left(\frac{\widehat{R}_c}{\sigma_s}\right)^{1/2}\int_{h+\delta_{n1}^*}^{h+\delta_{n2}^*}\left[1-(1-K)\frac{ln\delta_{n2}^* - ln(2\epsilon) - ln(2\widehat{R}_c) - 2ln\delta_n^* + ln\left(a_l^*b_l^*\right)}{(ln\delta_{n2}^* - ln\delta_{n1}^*) - (ln(2\epsilon) - ln(\beta/2))}\right]$$
$$\times\left\{\left[2\epsilon\delta_n^* - \beta\delta_n^*/2\right]\times\left[-2\left(\frac{\delta_n^*-\delta_{n1}^*}{\delta_{n2}^*-\delta_{n1}^*}\right)^3 + 3\left(\frac{\delta_n^*-\delta_{n1}^*}{\delta_{n2}^*-\delta_{n1}^*}\right)^2\right] + \beta\delta_n^*\Big/2\right\}\phi^*(z_s^*)dz_s^* + \frac{3\pi H}{\widehat{E}_c}\left(\frac{\widehat{R}_c}{\sigma_s}\right)^{1/2}\int_{h+\delta_{n2}^*}^{\infty}(z_s^*-h)\phi^*(z_s^*)dz_s^* \tag{47}$$

$$\beta^* = \beta\int_h^{h+\delta_{n1}^*}(z_s^*-h)\phi^*(z_s^*)dz_s^* + \beta\int_{h+\delta_{n1}^*}^{h+\delta_{n2}^*}(z_s^*-h)\phi^*(z_s^*)dz_s^* + \int_{h+\delta_{n1}^*}^{h+\delta_{n2}^*}2(z_s^*-h)[2\epsilon-\beta/2]\times\left[-2\left(\frac{\delta_n^*-\delta_{n1}^*}{\delta_{n2}^*-\delta_{n1}^*}\right)^3 + 3\left(\frac{\delta_n^*-\delta_{n1}^*}{\delta_{n2}^*-\delta_{n1}^*}\right)^2\right]\phi^*(z_s^*)dz_s^*$$
$$+4\epsilon\int_{h+\delta_{n2}^*}^{\infty}(z_s^*-h)\phi^*(z_s^*)dz_s^* \tag{48}$$

in which $\delta_{n1}^* = \frac{\delta_{n1}}{\sigma}$, $\delta_{n2}^* = \frac{\delta_{n2}}{\sigma}$, K= maximum contact pressure factor, $a_l^*b_l^* = \frac{a_lb_l}{\sigma_s^2}$, ϵ and a_lb_l can be calculated as follows

$$\epsilon = \frac{\mathbb{E}(e^2)e^2}{2(1-e^2)^{0.5}[\mathbb{E}(e^2) - \mathbb{K}(e^2)(1-e^2)]} \tag{49}$$

$$a_lb_l = 2\epsilon\widehat{R}_c\delta_nC \tag{50}$$

$$C = \frac{k_l\left[2-\frac{\delta_{n1}}{\delta_n}(2-\varsigma)\right] + 2\frac{\delta_{n1}}{\delta_n}\left(1-\frac{\delta_{n1}}{\delta_n}\right)}{(k_l-1)+\frac{\delta_{n1}}{\delta_n}} \tag{51}$$

where k_l is the constant of proportionality [98] and ς is as follows

$$\varsigma = \frac{2(\mathbb{E}(e^2) - \mathbb{K}(e^2)(1-e^2))}{\mathbb{K}(e^2)e^2} \tag{52}$$

In order to solve integrals in eqs. (47) and (48), Taylor expansion can be employed for $\phi^*(z_s^*)$ as follows [7]:

$$\phi^*(z_s^*) = \frac{1}{\sqrt{2\pi}}\left(1 - \frac{z_s^{*2}}{2} + \frac{z_s^{*4}}{8} - \frac{z_s^{*6}}{48} + \frac{z_s^{*8}}{384} + O(10)\right) \tag{53}$$

2.6. Energy-based normal contact

There are other models not based on Hertz theory and the assumption of elliptical contact. The energy-based theoretical formulation was introduced to calculate the magnitude and direction of contact normal forces as well as reference contact position [78,79]. The common concept of penalty methods for bodies in contact was utilised in which a

with respect to $\mathbf{x}_p$, $\|\mathbf{F}_n\|$ is the magnitude of normal force in the direction of normal vector $\mathbf{n}$, and θ is the rotational angle with respect to the original position. The different selection for energy function may range from linear to power formula.

The normal force magnitude is dependent on the selection of energy function forms. A few possible option for energy functions and the corresponding penalty coefficients is introduced in [78].

3. Tangential contact force models between non-spherical particles

3.1. Cattaneo-Mindlin-Deresiewicz (CMD) theory of tangential contact forces

3.1.1. Constant normal force and increasing tangential force

As shown in Fig. 10, for two particles in contact subjected to an initial normal contact force F_n, according to the postulation of Hertz-Mindlin [32] theory, an incremental tangential force, F_t, being applied in the x'-direction makes an angle θ pertinent to the principal axes of the elliptical contact area, as shown in Fig. 11. The following assumptions are applied to the Cattaneo-Mindlin-Deresiewicz (CMD) tangential contact model [99]:

(1) The normal pressure acting on the elliptical contact area aligns with Hertz normal contact theory. In other words, once the elliptical contact area undergoes tangential traction, both the size of the contact area and the normal pressure will be unchanged. Further, there is no interaction between the normal displacement calculated using Hertz theory and tangential traction.

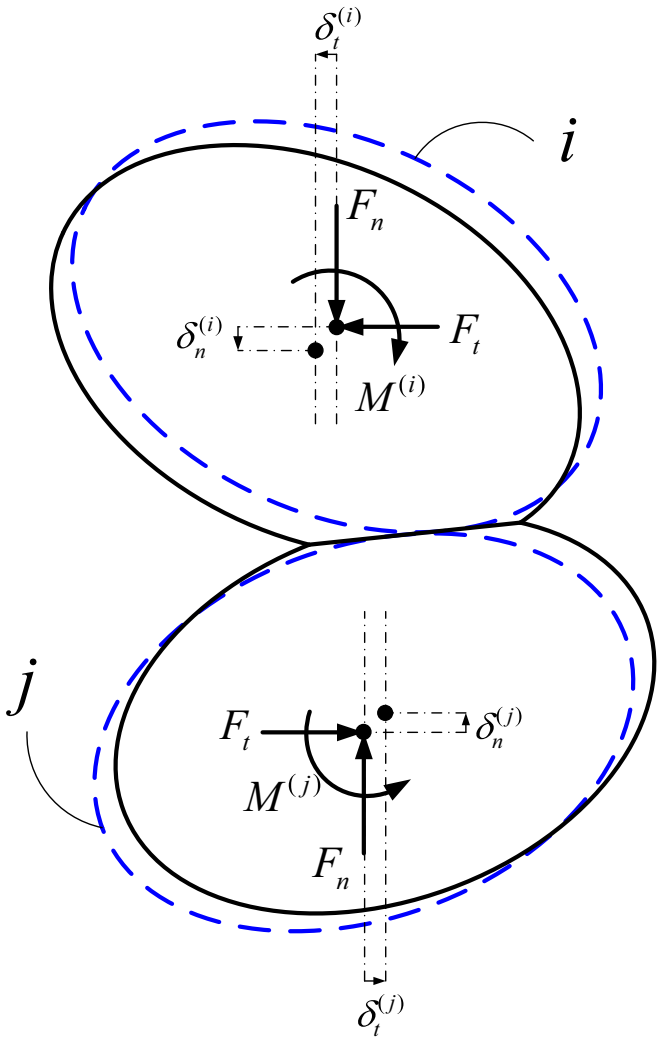

Fig. 10. Two arbitrary-shaped bodies in contact subjected to normal and tangential force.

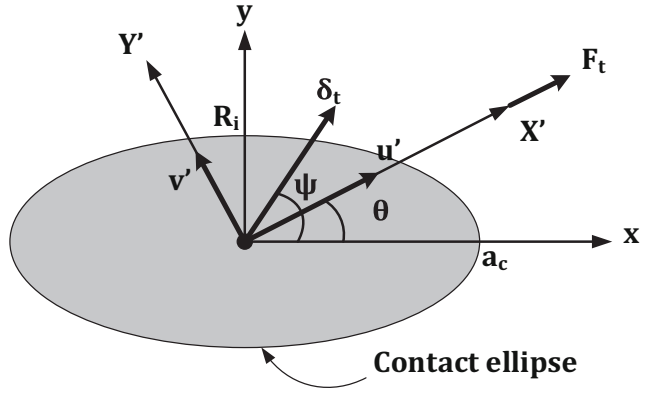

Fig. 11. Elliptical contact area of arbitrary-shaped bodies under applied tangential force.

(2) Slip takes place in the direction of the applied tangential force, which is triggered at the outer edge of the contact and develops inward over an annular area whose inner boundary is homothetic with the ellipse of the contact [100].
(3) Coulomb's law of sliding friction governs the behaviour of each point at the area of slip.
(4) The resultant tangential component of traction is in the direction of the applied force.

It is well recognised that the slip on the elliptical contact area must take place to maintain the assumption of finite traction at the outer edge of contact area [32]. Therefore, two cases can be detected for tangential slip as (1) no-slip case and (2) micro-slip case.

For no-slip cases, due to symmetry, the contact surface displacement in its plane occurs as a rigid body motion [101]. The resulting boundary value problem was solved by Mindlin [32], in which the tangential component of contact surface traction was denoted as a function of a relative displacement of a point (δ_t) in one particle far from the contact area with respect to a counterpart point in the other particle. For rigid particles with relatively small deformation, the two points can be assumed to be the mass centres of the two contacting particles, as shown in Fig. 10. The relation between the tangential force and the relative tangential displacement of two mass central points, can be given as [102]:

$$F_t = 2\pi G a_c \delta_t \chi \tag{56}$$

$$\chi = \left\{ \left[(1-\upsilon)\mathbb{K}(e^2) + \upsilon\mathbb{D}(e^2) \right]^2 cos^2\theta + \left[\mathbb{K}(e^2) - \upsilon\mathbb{D}(e^2) \right]^2 sin^2\theta \right\}^{-1/2} \tag{57}$$

Note here only the semi-major of the contact ellipse R_j is used in the calculation of F_t, which however should be accurately calculated by Eq. (3) for non-spherical particles. The angle between δ_t and the contact path major axis is denoted as ψ, which can be calculated as:

$$\psi = \text{atan}\left[\frac{\mathbb{K}(e^2) - \upsilon\mathbb{D}(e^2)}{(1-\upsilon)\mathbb{K}(e^2) + \upsilon\mathbb{D}(e^2)} tan\theta \right] \tag{58}$$

Under no slip condition, the magnitude of the force increases to infinity at the edge of the contact surface. This singularity in the traction violates physics law and therefore, slip occurs regardless of the magnitude of the applied tangential force [101].

For micro-slip cases, the initiation of slip at the edge of the contact rationalises the non-singular traction over the contact area. The tangential force-displacement relationship can be obtained as:

$$F_t = \mu F_n \left[1 - \left\{ 1 - \frac{4\pi G a_c}{3\mu F_n} \delta_t \chi \right\}^{3/2} \right] \tag{59}$$

Deresiewicz [103] showed that under special conditions when $\theta = 0$ and $\theta = \pi/2$, Eq. (59) can be simplified as

$$F_t = \mu F_n \left[1 - \left\{ 1 - \frac{16 \widehat{G} a_c}{3\mu F_n \Phi} \delta_t \right\}^{3/2} \right] \tag{60}$$

$$\Phi = \begin{cases} \frac{4}{\pi(2-\upsilon)} \left[(1-\upsilon)\mathbb{K}(e^2) + \upsilon\mathbb{D}(e^2) \right] \text{ for } \theta = 0 \\ \frac{4}{\pi(2-\upsilon)} \left[\mathbb{K}(e^2) - \upsilon\mathbb{D}(e^2) \right] \text{ for } \theta = \pi/2 \end{cases} \tag{61}$$

in which $\widehat{G} = \left(\sum_{i=1}^{2} \left(\frac{2-\upsilon_i}{G_i} \right) \right)^{-1}$ and G_i is the shear modulus of particles

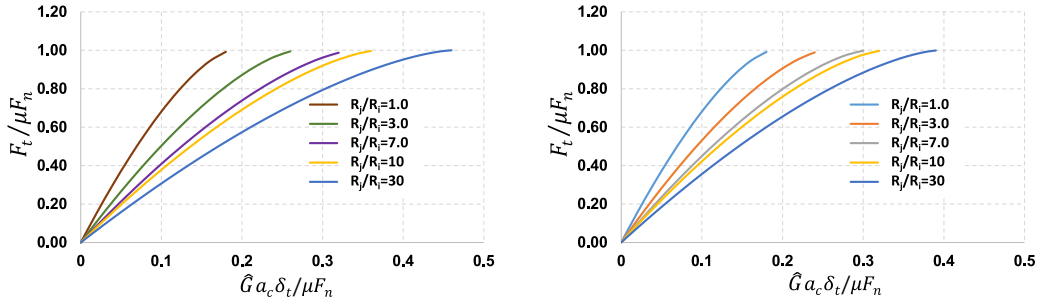

(a) $\theta = 0$ **(b) $\theta = \pi/2$**

Fig. 12. Variation of normalised shear force versus normalised shear displacement ($\upsilon = 0.3$).

in touch. Variation of normalised shear force versus normalised shear displacement is shown in Fig. 12. F_t will deflect up to $F_t = \mu F_n$ and eq. (60) gives the limit deflection, δ_{Li}^t

$$\delta_{Li}^t = \frac{3\mu F_n}{16\widehat{G}a_c}\Phi = \frac{\mu\widehat{E}_c\widehat{R}_c^{1/2}\delta_n^{3/2}}{4\widehat{G}a_c}\gamma\Phi \tag{62}$$

By simplifying the eq. (62), the limit deflection can be given as [104]:

$$\delta_{Li}^t = \frac{\pi\mu\widehat{E}_c\Phi}{8\widehat{G}\mathbb{K}(e^2)}\delta_n \tag{63}$$

Mindlin [32] computed the ratio of the initial tangential to the normal compliance for non-spherical particles as

$$\Re = \frac{\frac{d\delta_t}{dF_t}}{\frac{d\delta_n}{dF_n}} = \begin{cases} \dfrac{\pi(2-\upsilon)}{4(1-\upsilon)}\dfrac{1}{\mathbb{K}(e^2)}\left[\dfrac{2\mathbb{K}(e^2)}{\pi} - \dfrac{\upsilon\mathbb{N}(e^2)}{2\pi^2(2-\upsilon)\left(1-\left(\frac{R_i}{R_j}\right)^2\right)^{1/2}}\right] & \text{for } \theta = 0 \\ \dfrac{\pi(2-\upsilon)}{4(1-\upsilon)}\dfrac{1}{\mathbb{K}(e^2)}\left[\dfrac{2\mathbb{K}(e^2)}{\pi} + \dfrac{\upsilon\mathbb{N}(e^2)}{2\pi^2(2-\upsilon)\left(1-\left(\frac{R_i}{R_j}\right)^2\right)^{1/2}}\right] & \text{for } \theta = \pi/2 \end{cases} \tag{64}$$

$$\mathbb{N}(e^2) = 4\pi\left[(2-e^2)\frac{\mathbb{K}(e^2)}{e} - \frac{2\mathbb{E}(e^2)}{e}\right] \tag{65}$$

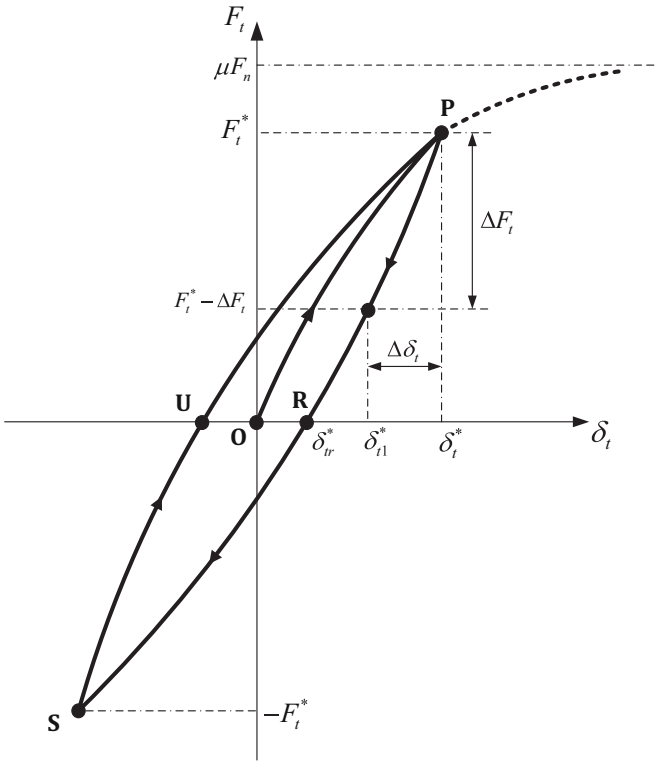

Fig. 13. Tangential force-displacement hysteresis loop for the case of normal constant load and oscillating tangential force [74].

3.1.2. Constant normal force and decreasing tangential force

Mindlin and Deresiewicz [101] further considered how the tangential force decreases from the maximum turning point values, F_t^*, for spherical particles. For no-slip conditions, the tangential traction on the edge of the contact area would be negative infinity. As a result, the slip might assume to take place, however, its direction will be in the opposite side of the initial slip.

For non-spherical bodies, the displacement of adhered region, δ_a, corresponding to the additional traction, can be similar to that of spherical particles with the correction factor Φ of eq. (61) included, given as [100].

$$\delta_a = -\frac{3\mu F_n(2-\upsilon)}{8Ga_c}\left[1-\left(1-\frac{F_t^* - F_t}{2\mu F_n}\right)^{\frac{2}{3}}\right]\Phi \tag{66}$$

Deresiewicz [100] derived the solution for the contact of a pair of non-spherical particles subjected to the decreasing tangential load started from F_t^*. The tangential displacement for this case is given by:

$$\delta_t = \frac{3\mu F_n(2-\upsilon)}{16Ga_c}\left[2\left(1-\frac{F_t^* - F_t}{2\mu F_n}\right)^{\frac{2}{3}} - \left(1-\frac{F_t^*}{\mu F_n}\right)^{\frac{2}{3}} - 1\right]\Phi \tag{67}$$

The tangential compliance during the unloading is

$$S = \frac{d\delta_t}{dF_t} = \frac{(2-\upsilon)}{4Ga_c}\left[\left(1-\frac{F_t^* - F_t}{2\mu F_n}\right)^{-\frac{1}{3}}\right]\Phi \tag{68}$$

3.1.3. Constant normal force and oscillating tangential force

Mindlin and Deresiewicz [101] showed that the successive increase of F_t from $-F_t^*$ to F_t^* will be similar to the reduction of F_t from F_t^* to $-F_t^*$ except for the sign reversal. Hence, the load-displacement curve forms a

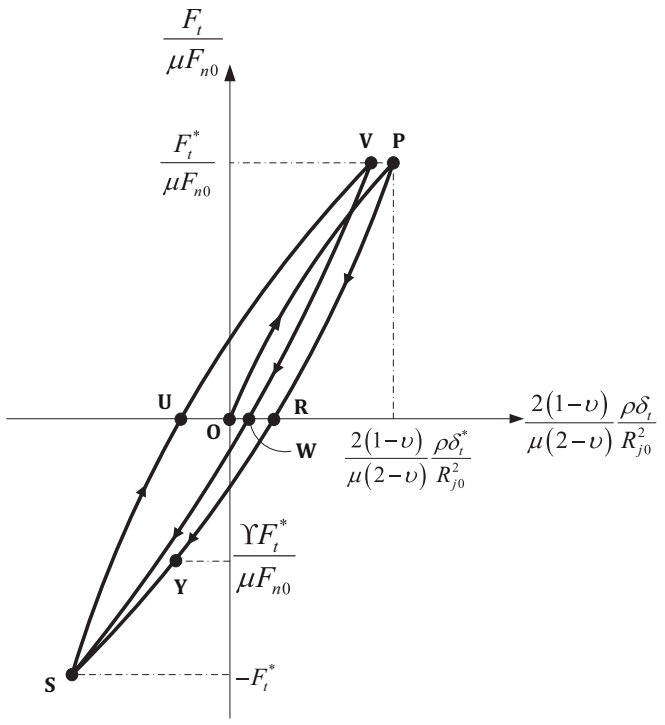

Fig. 14. Theoretical hysteresis loop due to oscillating normal and tangential force having constant direction [103].

closed-loop, and this path will be navigated in the course of successive oscillation of F_t between the limits $\pm F_t^*$, provided F_n is kept constant. The relationship between tangential force and tangential displacement is schematically depicted in Fig. 13 for the case of constant normal force. As seen, the residual displacement of δ_{tr}*emerges when the tangential force is completely removed, i.e., $F_t = 0$, in the F_t-decreasing regime of the loading history and this residual displacement can be vanished by applying a tangential force in the reverse direction. This phenomenon is the result of energy dissipation, which makes a hysteresis tangential force-displacement curve with the same amount of energy loss in the course of each complete loading cycle [74]. The enclosed area in the loop (i.e., OPRSU loop in Fig. 13) denotes the frictional energy dissipated in each cycle of loading as

$$E_d = \frac{9(2-\upsilon)(\mu F_n)^2}{10Ga_c}\left[1-\left(1-\frac{F_t^*}{\mu F_n}\right)^{\frac{5}{3}}-\frac{5F_t^*}{6\mu F_n}\left(1+\left(1-\frac{F_t^*}{\mu F_n}\right)^{\frac{2}{3}}\right)\right]\Phi \tag{69}$$

3.1.4. Oblique forces (varying normal tangential force)

Generally, once granular particles undergo varying external forces, the inter-particle contact surfaces are subjected to variable normal and tangential forces. The tangential compliance between spheres in contact, initially subjected to F_{n0} and additional normal and tangential forces with increasing rates were calculated by Mindlin and Deresiewicz [101] and extended to non-spherical bodies by Deresiewicz [100] as

$$S = \begin{cases} \frac{(2-\upsilon)}{4Ga_c}\left[\mu\frac{dF_n}{dF_t}+\left(1-\mu\frac{dF_n}{dF_t}\right)\left(1-\frac{F_t}{\mu F_n}\right)^{-\frac{1}{3}}\right]\Phi & \text{for } 0 \le \frac{dF_n}{dF_t} \le \frac{1}{\mu} \\ \frac{(2-\upsilon)}{4Ga_c}\Phi & \text{for } \frac{dF_n}{dF_t} > \frac{1}{\mu} \end{cases} \tag{70}$$

Varying oblique force can be given to a pair of non-spherical particles under an initial normal force F_{n0} and a tangential force F_t^* and then the tangential force is reduced to F_t, while the normal force changes at an increasing rate. The tangential compliance for this case is [101]:

$$S = \begin{cases} \frac{(2-\upsilon)}{4Ga_c}\left[\mu\frac{dF_n}{dF_t}+\left(1-\mu\frac{dF_n}{dF_t}\right)\left(1-\frac{F_t^*-F_t}{2\mu F_n}\right)^{-\frac{1}{3}}\right]\Phi & \text{for} -\frac{1}{\mu} \le \frac{dF_n}{dF_t} < 0 \\ \frac{(2-\upsilon)}{4Ga_c}\Phi & \text{for} \frac{dF_n}{dF_t} \le -\frac{1}{\mu} \end{cases} \tag{71}$$

3.1.5. Oscillating normal and tangential force

The other loading status which is of interest in granular media is the oscillating normal and tangential force. Let us assume that a pair of non-spherical particles initially compressed with a normal force F_{n0}.The contact major semiaxis radius is R_{j0}. Then the particles are subjected to additional normal and tangential forces whose resultant, ρ, oscillates in magnitude but along a constant direction. It is assumed that the tangential component oscillates between $\pm F_t^*$, while the normal component variation maintains a constant value for dF_n/dF_t. Mindlin and Deresiewicz [101] and Deresiewicz [103] assumed that the hysteresis loop for the force-displacement curve has three identified parts, shown in Fig. 14, as (1) loading (2) unloading (3) stabilised loading/unloading. The load-displacement curve in Fig. 14 after sweeping the curve OPRYS, stabilises along the path SUVWS. The tangential compliance in the course of initial loading (i.e., along path OP) is denoted as

$$S = \frac{(2-\upsilon)}{4Ga_c}\left[\Theta+(1-\Theta)\left(1-\frac{\Lambda}{1+\Theta\Lambda}\right)^{-1/3}\right]\Phi \tag{72}$$

and during initial unloading (i.e., along path PRY and YS)

$$S = \begin{cases} \frac{(2-\upsilon)}{4Ga_c}\left\{-\Theta+(1+\Theta)\left[1-(1-\Theta)\frac{\Lambda^*-\Lambda}{2(1+\Theta\Lambda)}\right]^{-1/3}\right\}\Phi & \text{for } \Upsilon\Lambda^* \le \Lambda < \Lambda^* \\ \frac{(2-\upsilon)}{4Ga_c}\left\{-\Theta+(1+\Theta)\left[1+\frac{1}{1+\Theta\Lambda}\right]^{-1/3}\right\}\Phi & \text{for } -\Lambda^* \le \Lambda < \Upsilon\Lambda^* \end{cases} \tag{73}$$

in which, $\Lambda = F_t/\mu F_{n0}$, $\Lambda^* = F_t^*/\mu F_{n0}$, $\Theta = \mu/\Xi$, $\Xi = dF_t/dF_n \ge \mu$, and $\Upsilon = (\Theta-1)/(\Theta+1) \le 0$.

The tangential compliance during the loading in the stabilised cycle (i.e., along path SUV) is

$$S = \frac{(2-\upsilon)}{4Ga_c}\left\{\Theta+(1-\Theta)\left[1-(1+\Theta)\frac{\Lambda^*+\Lambda}{2(1+\Theta\Lambda)}\right]^{-1/3}\right\}\Phi \tag{74}$$

The tangential compliance associated with the stabilised unloading (i.e., along path VWS) can be calculated using Eq. (74) by reversing the signs of Θ and Λ. The energy loss attributed to each cycle is denoted by

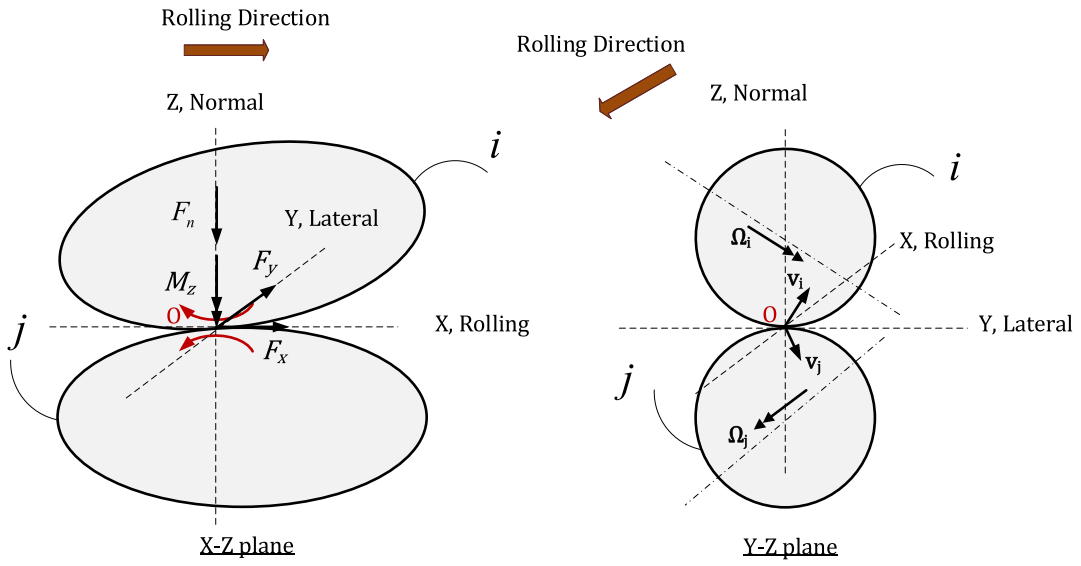

Fig. 15. Particles rolling over each other.

Table 4
List of models for calculating normal contact force.

Contact force model	Equations	Details
Elastic regime ($\delta_n < \delta_{n1}$)		
General Equations	Smooth contact: $F_n = \frac{4}{3}\widehat{E}_c\widehat{R}_c^{1/2}\delta_n^{3/2}\gamma$ $A_n = \pi\widehat{R}_c\delta_n\beta$ Non-smooth contact: $F_n = \frac{4}{3}NA_n\widehat{E}_c\widehat{R}_c^{1/2}\sigma_s^{3/2}\gamma^*$ $A_n = \pi NA_n\widehat{R}_c\sigma_s\beta^*$	See Eqs. (1) and (2); $\widehat{R}_c$ defined in Eqs. (3)–(5); γ or γ^* and β or β^* are correction factors which will be different when considering different situations.
Smooth, non-adhesive, Hertz [25]	$\gamma = \frac{\pi\sqrt{2}(\mathbb{E}(e^2))^{0.5}}{2(\mathbb{K}(e^2))^{1.5}(1-e^2)^{0.5}}$ $\beta = \frac{2\mathbb{E}(e^2)}{\mathbb{K}(e^2)(1-e^2)^{0.5}}$	e^2 is the elliptical contact eccentricity, see Eqs. (13) and (14).
Smooth, adhesive, JKR [63]	$\gamma = \frac{3\pi\sqrt{2}}{2}\frac{\frac{\Pi_1-\Pi_2 g^{5/2}}{1-g^{1/2}} - \frac{1}{3}(\Pi_2 g^2+\Pi_1)}{\left(2\mathbb{K}(e^2)\frac{\Pi_1-\Pi_2 g^{5/2}}{1-g^{1/2}} - \Pi_1\mathbb{B}(e^2) - g^2\Pi_2\mathbb{D}(e^2)\right)^{3/2}}$ $\beta = \frac{2g}{\mathbb{K}(e^2)\frac{\Pi_1-\Pi_2 g^{5/2}}{1-g^{1/2}} - \Pi_1\mathbb{B}(e^2) - g^2\Pi_2\mathbb{D}(e^2)}$	$e^2 = 1-g^2$ See Eqs. (23)–(27) for the integrals in the equations.
Non-smooth, GW, adhesive or non-adhesive [48]	$\gamma^* = \gamma\frac{1}{4\sqrt{\pi}}exp\left(\frac{-h^2}{4}\right)\sqrt{h}\left[\left(h^2+1\right)\mathscr{K}_{1/4}\left(\frac{h^2}{4}\right) - h^2\mathscr{K}_{3/4}\left(\frac{h^2}{4}\right)\right]$ $\beta^* = \beta\left(\frac{1}{\sqrt{2\pi}}exp\left(\frac{-h^2}{4}\right) - \frac{1}{2}herf\left(\frac{h}{\sqrt{2}}\right)\right)$	
Elastic-plastic or fully Plastic regime ($\delta_n \geq \delta_{n1}$)		
Elastic-Plastic contact, Jamari et al. [93]	$F_{n-EP} = A_{n-EP}\left[c_hH - H\left(c_h - \frac{2}{3}K_v\right)\frac{ln\delta_{n2} - ln\delta_n}{ln\delta_{n2} - ln\delta_{n1}}\right]$ $A_{n-EP} = \pi\widehat{R}_c\delta_n\beta +$ $\left(2\pi(R_iR_j)^{0.5}\delta_n - \pi\widehat{R}_c\delta_n\beta\right)\left[3\left(\frac{\delta_n-\delta_{n1}}{\delta_{n2}-\delta_{n1}}\right)^2 - 2\left(\frac{\delta_n-\delta_{n1}}{\delta_{n2}-\delta_{n1}}\right)^3\right]$	$\delta_{n2} > \delta_n \geq \delta_{n1}$
Fully Plastic contact, Jamari et al. [93]	$F_n = 2\pi\delta_n(R_iR_j)^{0.5}c_hH$ $A_n = 2\pi(R_iR_j)^{0.5}\delta_n$	$\delta_n \geq \delta_{n2}$
Dissipative force		
Smooth, non-adhesive, Brilliantov [75]	$\mathbf{F_{n-dis}} = 2A\widehat{E}_c\widehat{R}_c^{1/2}\delta_n^{1/2}\dot{\delta}_n\gamma\mathbf{n}$	
Smooth, adhesive, Brilliantov [90]	$\mathbf{F_{n-dis}} = \left(2A\widehat{E}_c\widehat{R}_c^{1/2}\delta_n^{1/2}\dot{\delta}_n\gamma + \frac{3}{4}B\sqrt{\frac{\pi\chi}{D}}\widehat{R}_c^{3/4}\dot{\delta}_n\delta_n^{-1/4}\right)\mathbf{n}$	

Table 5
List of models for calculating tangential contact force.

Contact force model	Contact status	Definition	Equations
CMD [96]	Increasing tangential contact under constant normal force	Smooth, elastic, non-adhesive, slip	$F_t = \mu F_n\left[1-\left\{1-\frac{16\widehat{G}R_j}{3\mu F_n\Phi}\delta_t\right\}^{3/2}\right]$ $\Phi = \begin{cases}\frac{4}{\pi(2-\upsilon)}\left[(1-\upsilon)\mathbb{K}(e^2)+\upsilon\mathbb{D}(e^2)\right] \text{ for } \theta=0\\ \frac{4}{\pi(2-\upsilon)}\left[\mathbb{K}(e^2)-\upsilon\mathbb{D}(e^2)\right] \text{ for } \theta=\pi/2\end{cases}$
	Decreasing tangential contact under constant normal force		$\delta_t = \frac{3\mu F_n(2-\upsilon)}{16GR_j}\left[2\left(1-\frac{F_t^*-F_t}{2\mu F_n}\right)^{\frac{2}{3}}-\left(1-\frac{F_t^*}{\mu F_n}\right)^{\frac{2}{3}}-1\right]\Phi$
Mindlin-Deresiewicz [101] Deresiewicz [100]	Increasing tangential contact under varying normal force		$S = \begin{cases}\frac{(2-\upsilon)}{4GR_j}\left[\mu\frac{dF_n}{dF_t}+\left(1-\mu\frac{dF_n}{dF_t}\right)\left(1-\frac{F_t}{\mu F_n}\right)^{-\frac{1}{3}}\right]\Phi & 0\le\frac{dF_n}{dF_t}\le\frac{1}{\mu}\\ \frac{(2-\upsilon)}{4GR_j}\Phi\frac{dF_n}{dF_t} & >\frac{1}{\mu}\end{cases}$
	Decreasing tangential contact under varying normal force		$S = \begin{cases}\frac{(2-\upsilon)}{4GR_j}\left[\mu\frac{dF_n}{dF_t}+\left(1-\mu\frac{dF_n}{dF_t}\right)\left(1-\frac{F_t^*-F_t}{2\mu F_n}\right)^{-\frac{1}{3}}\right]\Phi & -\frac{1}{\mu}\le\frac{dF_n}{dF_t}<0\\ \frac{(2-\upsilon)}{4GR_j}\Phi\frac{dF_n}{dF_t} & \le-\frac{1}{\mu}\end{cases}$
Mindlin [32]		Smooth, elastic, non-adhesive, no slip	$F_t = 2\pi GR_j\delta_t\chi$ $\chi = \left\{\left[(1-\upsilon)\mathbb{K}(e^2)+\upsilon\mathbb{D}(e^2)\right]^2\cos^2\theta+\left[\mathbb{K}(e^2)-\upsilon\mathbb{D}(e^2)\right]^2\sin^2\theta\right\}^{-1/2}$
Hisakado- Tsukioze [105]	Increasing tangential contact	Non-smooth, elastic, non-adhesive, no slip	$F_t = 2\pi NA_nG\delta_t\sqrt{R_j\sigma}\chi^*$ $\chi^* = \frac{\chi\sqrt{\pi}}{4\sqrt{2h}}exp\left(-\frac{h^2}{4}\right)\left\{-h^2\mathscr{I}_{-1/4}\left(\frac{h^2}{4}\right)+\left(h^2+2\right)\mathscr{I}_{\frac{1}{4}}\left(\frac{h^2}{4}\right)+h^2\left(-\mathscr{I}_{\frac{3}{4}}\left(\frac{h^2}{4}\right)+\mathscr{I}_{\frac{5}{4}}\left(\frac{h^2}{4}\right)\right)\right\}$
Dissipative force			
	Increasing tangential contact	Smooth, elastic, non-adhesive, slip	$F_{t-dis} = \frac{\eta_1}{2G}\dot{\delta}_t\frac{\partial F_t}{\partial\delta_t} = \frac{4\eta_1\dot{\delta}_tR_j}{\Phi}\left\{1-\frac{16\widehat{G}R_j}{3\mu F_n\Phi}\delta_t\right\}^{1/2}$

$$E_d = \frac{9(2-\upsilon)(\mu F_{n0})^2}{10Ga_{c0}}\left[\frac{1}{4\Theta}\left(-\frac{1}{\Upsilon}(1-\Theta\Lambda^*)^{\frac{5}{3}}+\Upsilon(1+\Theta\Lambda^*)^{\frac{5}{3}}\right)-\frac{1}{1-\Theta^2}(1-\Lambda^*)^{\frac{2}{3}}\left(1-\frac{1+5\Theta^2}{6}\Lambda^*\right)\right]\Phi \tag{75}$$

For small values of Λ*the energy loss can be calculated as

$$E_d = \frac{(2-\upsilon)(F_t^*)^3}{36Ga_{c0}\mu F_{n0}}(1-\Theta^2)\Phi \tag{76}$$

3.1.6. Mindlin theory of twisting couples

A pair of particles can experience specific types of loading, which results in twisting moments around the line of contact of centres of curvature of the adjoining parts of bodies. To address this type of contact problem, Mindlin [32] assumed that a pair of particles compressed by a normal force and then a twisting couple around the normal force axis increases monotonically to a specific value of M_t. It was recognised that for no-slip contact status, the contact surface experiences rigid-body rotation around the contact centreline and the circumferential shearing stress shows a vertical asymptote at the edge of the contact. Assuming no-slip condition, the torsional compliance for general non-spherical contact is given as [32]:

$$C_\tau = \frac{d\theta_t}{dM_t} = \frac{3}{8\mu R_i^3}\left[\frac{8(\mathbb{B}(e^2)\mathbb{D}(e^2)-\nu\mathbb{C}(e^2)\mathbb{E}(e^2))}{\pi(\mathbb{E}(e^2)-4\nu(1-e^2)\mathbb{C}(e^2))}\right] \tag{77}$$

where θ_t is the twisting angle of rotation. With the same hypotheses as those made for the tangential contact force, the slip in a circumferential direction at the edge of the contact area over the ring-shaped area occurs to maintain physical law, and the rest of the contact portion undergoes rigid-body rotation around contact centreline.

3.2. Tangential contact of rough particles

According to the theory of Hisakado and Tsukioze [105], the elastic tangential displacement of an asperity in contact with an infinitely rigid smooth surface under a tangential force is given as

$$\delta_t = \frac{2-\upsilon}{2\pi G}\frac{F_{tk}}{a_k} \tag{78}$$

where a_k is the radius of the Hertzian contact area of asperity k with an infinitely rigid surface and F_{tk} is the tangential force of the asperity k. The total tangential force that can be supported by n asperities will be [106]:

$$\delta_t = \sum_{k=1}^{n} F_{tk} \tag{79}$$

For non-spherical particles with an elliptical contact area, by considering Eq. (56), Eq. (78) can be rewritten as

$$F_t = 2\pi G\delta_t\chi\sum_{k=1}^{n} a_k \tag{80}$$

The radius of the contact area of an asperity can be written as

$$a_k = \sqrt{(z_s-d)a_c} \tag{81}$$

Therefore, the radius of the contact area of all asperity curvatures at height z will be

$$\sum_{k=1}^{n} a_k = NA_n\sqrt{a_c\sigma}\int_h^\infty\left(z_s^*-h\right)^{1/2}\phi^*\left(z_s^*\right)dz_s^* \tag{82}$$

The tangential contact force for rough surface can be expressed as follows:

Table 6
List of models for calculating rolling contact force and moment.

Rolling contact model	Equations	Details
Linear theory [108]	$F_x = -(a_c b_c)^2 \widehat{G} c_{11} \xi_x$ $F_y = -(a_c b_c)^2 \widehat{G} c_{22} \xi_y - (a_c b_c)^3 \widehat{G} c_{23} \varphi$ $M_z = (a_c b_c)^3 \widehat{G} c_{23} \xi_y - (a_c b_c)^4 \widehat{G} c_{33} \varphi$	See Eqs. (86)–(88)
Nonlinear theory [109]	$\xi_x = -\frac{3\mu F_n}{a_c b_c G c_{11}} \left(\frac{F_x}{F_t}\right) \left[1 - \left(1 - \frac{F_t}{\mu F_n}\right)^{1/3}\right]$ $\xi_y = -\frac{3\mu F_n}{a_c b_c G c_{22}} \left(\frac{F_y}{F_t}\right) \left[1 - \left(1 - \frac{F_t}{\mu F_n}\right)^{1/3}\right]$	See Eqs. (92) and (93)

$$F_t = 2\pi N A_n G \delta_t \sqrt{a_c \sigma} \chi^* \tag{83}$$

$$\chi^* = \frac{\chi\sqrt{\pi}}{4\sqrt{2h}} exp\left(-\frac{h^2}{4}\right)\left\{-h^2 \mathscr{I}_{-1/4}\left(\frac{h^2}{4}\right) + \left(h^2+2\right)\mathscr{I}_{\frac{1}{4}}\left(\frac{h^2}{4}\right) + h^2\left(-\mathscr{I}_{\frac{3}{4}}\left(\frac{h^2}{4}\right) + \mathscr{I}_{\frac{5}{4}}\left(\frac{h^2}{4}\right)\right)\right\} \tag{84}$$

3.3. Tangential dissipative force

Similar to normal force the dissipative force between viscoelastic particles can be calculated using the following equation [107]:

$$F_{t-dis} = \frac{\eta_1}{2G}\dot{\delta}_t \frac{\partial F_t}{\partial \delta_t} = \frac{4\eta_1 \dot{\delta}_t a_c}{\Phi}\left\{1 - \frac{16\widehat{G} a_c}{3\mu F_n \Phi}\delta_t\right\}^{1/2} \tag{85}$$

4. Rolling contact model between non-spherical particles

4.1. Kalker's linear rolling contact theory

In the linear theory of rolling contact proposed by Kalker [108], the tangential forces and moment at the contact point are linear function of the longitudinal, lateral, and spin creepage. For non-spherical particles with hertzian contact area, where the rolling is assumed to occur along one of the principal axes of the contact ellipse, x-axis in Fig. 15., the total tangential force, F_x and F_y, and the moment around the z-axis, M_z, have the following form:

$$F_x = -(a_c b_c)^2 \widehat{G} c_{11} \xi_x \tag{86}$$

$$F_y = -(a_c b_c)^2 \widehat{G} c_{22} \xi_y - (a_c b_c)^3 \widehat{G} c_{23} \varphi \tag{87}$$

$$M_z = (a_c b_c)^3 \widehat{G} c_{23} \xi_y - (a_c b_c)^4 \widehat{G} c_{33} \varphi \tag{88}$$

where c_{ij} is tabulated in [108] for exact values. Alternatively, the theories of Vermeulen-Johnson [109] may be used to obtain approximate analytical solutions for c_{11}, c_{22}, and c_{32}. ξ_x, ξ_y, and φ are longitudinal (in rolling direction), lateral, and spin creepages of particle i with respect to particle j, given by

$$\xi_x = \frac{\left[v_{ix} - v_{jx} - \left(R_{ix}\Omega_{iy} + R_{jx}\Omega_{jy}\right)\right]}{\overline{V}} \tag{89}$$

$$\xi_x = \frac{\left[v_{iy} - v_{jy} - \left(\frac{\Omega_{ix}}{\Omega_{iy}} - \frac{\Omega_{jx}}{\Omega_{jy}}\right)\overline{V}\right]}{\overline{V}} \tag{90}$$

$$\varphi = \frac{\left(\Omega_{iz} - \Omega_{jz}\right)}{\overline{V}} \tag{91}$$

where $\mathbf{\Omega_i} = (\Omega_{ix}, \Omega_{iy}, \Omega_{iz})$ and $\mathbf{\Omega_j} = (\Omega_{jx}, \Omega_{jy}, \Omega_{jz})$ are angular velocity vectors of particles i and j, respectively, $\mathbf{V_i} = (v_{ix}, v_{iy}, v_{iz})$ and $\mathbf{V_j} = (v_{jx}, v_{jy}, v_{jz})$ are translational velocity vectors of particles i and j, respectively, and $\overline{V}$ is the rolling velocity. R_{ix} and R_{jx} are radii of curvature at contact point for particle i and j, respectively.

4.2. Vermeulen-Johnson nonlinear rolling contact theory

In this theory [109], the contact area is split into two zones, (1) the zone of adhesion where no slip occurs, and (2) the zone of slip. It is assumed that the adhesion zone is elliptic with the same orientation of the axes as the contact ellipse and with the same ratio of the axes. The relation between longitudinal and lateral creepage and tangential force read as

$$\xi_x = -\frac{3\mu F_n}{a_c b_c G c_{11}} \left(\frac{F_x}{F_t}\right) \left[1 - \left(1 - \frac{F_t}{\mu F_n}\right)^{1/3}\right] \tag{92}$$

$$\xi_y = -\frac{3\mu F_n}{a_c b_c G c_{22}} \left(\frac{F_y}{F_t}\right) \left[1 - \left(1 - \frac{F_t}{\mu F_n}\right)^{1/3}\right] \tag{93}$$

5. Conclusions

This paper provides an extensive review of the current analytical contact force models for the simulation of non-spherical particles under normal and tangential contact regimes. The review focuses on providing more accurate contact force models, though more complicated than the current ones, to the DEM community. Several factors in the contact models are considered such as material constitutive laws (e.g., elastic, viscoelastic, and elastic-plastic behaviour), applied load regime (e.g., either normal or tangential), surface friction and adhesion (e.g., smooth, non-smooth, and adhesive). Numerical results have shown that based on the accurate geometrical model, the effect of surface properties on the predicted contact force and contact area is obvious, which may further exaggerate the errors caused by using simplified contact force models for non-spherical particles [10]. Finally, a list of equations recommended for calculating elliptical contact force in normal and tangential directions and rolling contact under different scenarios are summarised in Table 4, Table 5 and Table 6, respectively. These force models can be used in DEM to predict forces and related particle dynamic behaviours more accurately, especially for non-spherical particles, non-smooth particles and adhesive particles.

Declaration of Competing Interest

None.

Data availability

Data will be made available on request.

Acknowledgments

The authors are grateful for the financial support from Australian Research Council (IH140100035) and JITRI (Jiangsu Industrial

Technology Research Institute).

References

[1] P. Wriggers, Computational Contact Mechanics, Wiley, Chichester, 2002.
[2] Q.J. Zheng, H.P. Zhu, A.B. Yu, Finite element analysis of the contact forces between a viscoelastic sphere and rigid plane, Powder Technol. 226 (2012) 130–142.
[3] G. Lu, J.R. Third, C.R. Muller, Discrete element models for non-spherical particle systems: from theoretical developments to applications, Chem. Eng. Sci. 127 (2015) 425–465.
[4] W.Q. Zhong, A.B. Yu, X.J. Liu, Z.B. Tong, H. Zhang, DEM/CFD-DEM modelling of non-spherical particulate systems: theoretical developments and applications, Powder Technol. 302 (2016) 108–152.
[5] H.Q. Ma, L.Y. Zhou, Z.H. Liu, M.Y. Chen, X.H. Xia, Y.Z. Zhao, A review of recent development for the CFD-DEM investigations of non-spherical particles, Powder Technol. 412 (2022).
[6] V.L. Popov, M. Heß, E. Willert, Handbook of Contact Mechanics : Exact Solutions of Axisymmetric Contact Problems, Springer Nature, 2019.
[7] M.H. Korayem, H. Khaksar, H.J. Sharahi, Modeling and simulation of contact parameters of elliptical and cubic nanoparticles to be used in nanomanipulation based on atomic force microscope, Ultramicroscopy. 206 (2019).
[8] C. Zeng, S. Moller-Tank, A. Asokan, B. Dragnea, Probing the link among genomic cargo, contact mechanics, and Nanoindentation in recombinant adeno-associated virus 2, J. Phys. Chem. B 121 (2017) 1843–1853.
[9] L. Wang, K.J. Dong, C.C. Wang, R.P. Zou, Z.Y. Zhou, A.B. Yu, Computer simulation of the packing of nanoparticles, Powder Technol. 401 (2022).
[10] K. Kildashti, K. Dong, B. Samali, An accurate geometric contact force model for super-quadric particles, Comput. Method. Appl. M. (2020) 360.
[11] K. Kildashti, K.J. Dong, B. Samali, Q.J. Zheng, A.B. Yu, Evaluation of contact force models for discrete modelling of ellipsoidal particles, Chem. Eng. Sci. 177 (2018) 1–17.
[12] B. Feeny, Guran As, N. Hinrichs, K. Popp, A historical review on dry friction and stick-slip phenomena, Appl. Mech. Rev. 51 (1998) 321–341.
[13] A.A. Shabana, Dynamics of Multibody Systems, 4 ed., Cambridge University Press, Cambridge, 2013.
[14] W.F. Sun, Q.H. Zeng, A.B. Yu, Calculation of noncontact forces between silica Nanospheres, Langmuir. 29 (2013) 2175–2184.
[15] W.F. Sun, Q.H. Zeng, A.B. Yu, Interaction forces between carbon nanospheres: a molecular dynamics simulation study, Chem. Eng. Sci. 121 (2015) 23–31.
[16] P. Yang, Q.H. Zeng, K.J. Dong, H.P. Zhu, A quick method for developing interparticle force models of spherical gold nanoparticles from molecular dynamics simulation, Powder Technol. 362 (2020) 501–506.
[17] W. Sextro, Dynamical Contact Problems with Friction : Models, Methods, Experiments, and Applications, Springer, New York, 2002.
[18] D.S. Simulia, Abaqus Analysis user's Manual, Dassault Syst. Pawtucket, USA, 2018.
[19] C.A. Brebbia, J. Dominguez, Boundary element methods for potential problems, Appl. Math. Model. 1 (1977) 372–378.
[20] T. Andersson, B.G. Allan-Persson, The boundary element method applied to two-dimensional contact problems, in: C.A. Brebbia (Ed.), Progress in Boundary Element Methods Vol. 2, New York, NY, Springer New York, 1983, pp. 136–157.
[21] G. Karami, A Boundary Element Method for Two-Dimensional Contact Problems, Springer-Verlag, Berlin, 1989.
[22] K.W. Man, Contact Mechanics Using Boundary Elements, Computational mechanics publications, Southampton, 1994.
[23] G.F. Dargush, A. Soom, Contact modeling in boundary element analysis including the simulation of thermomechanical wear, Tribol. Int. 100 (2016) 360–370.
[24] G.M.L. Gladwell, Contact Problems in the Classical Theory of Elasticity. Alphen aan den Rijn, the Netherlands, Sijthoff & Noordhoff, Germantown, Md, 1980.
[25] K.L. Johnson, Contact Mechanics, Cambridge University Press, Cambridge, 1985.
[26] H.A. Francis, A finite surface element model for plane-strain elastic contact, Wear. 76 (1982) 221–245.
[27] N. Ren, S.C. Lee, Contact simulation of three-dimensional rough surfaces using moving grid method, J. Tribol. 115 (1993) 597–601.
[28] P.A. Cundall, O.D.L. Strack, A discrete numerical model for granular assemblies, Geotechnique. 29 (1979) 47–65.
[29] D.A. Hills, D. Nowell, A. Sackfield, Mechanics of Elastic Contacts, Butterworth-Heinemann, Oxford [England]; Boston, 1993.
[30] N. Hinrichs, M. Oestreich, K. Popp, On the modelling of friction oscillators, J. Sound Vib. 216 (1998) 435–459.
[31] M. Ciavarella, The generalized Cattaneo partial slip plane contact problem. I - theory, Int. J. Solids Struct. 35 (1998) 2349–2362.
[32] R.D. Mindlin, Compliance of elastic bodies in contact, J. Appl. Mech-T Asme. 16 (1949) 259–268.
[33] H. Hertz, Ueber die Berührung fester elastischer Körper, J. Reine Angewandte Mathematik (Crelle's Journal) 92 (1882) 156–171.
[34] J. Jäger, Elastic contact of equal spheres under oblique forces, Arch. Appl. Mech. 63 (1993) 402–412.
[35] H.P. Zhu, A.B. Yu, A theoretical analysis of the force models in discrete element method, Powder Technol. 161 (2006) 122–129.
[36] P.A. Langston, U. Tuzun, D.M. Heyes, Discrete element simulation of granular flow in 2d and 3d hoppers - dependence of discharge rate and wall stress on particle interactions, Chem. Eng. Sci. 50 (1995) 967–987.
[37] P.W. Cleary, M.L. Sawley, DEM modelling of industrial granular flows: 3D case studies and the effect of particle shape on hopper discharge, Appl. Math. Model. 26 (2002) 89–111.
[38] T. Elperin, E. Golshtein, Comparison of different models for tangential forces using the particle dynamics method, Phys. A. 242 (1997) 332–340.
[39] O.R. Walton, R.L. Braun, Viscosity, granular-temperature, and stress calculations for shearing assemblies of inelastic, frictional disks, J. Rheol. 30 (1986) 949–980.
[40] A. Ovcharenko, G. Halperin, I. Etsion, Experimental study of adhesive static friction in a spherical elastic-plastic contact, J. Tribol-T Asme. (2008) 130.
[41] S. Maegawa, F. Itoigawa, T. Nakamura, Optical measurements of real contact area and tangential contact stiffness in rough contact interface between an adhesive soft elastomer and a glass plate, J. Adv. Mech. Des. Syst. (2015) 9.
[42] R.S. Dwyer-Joyce, B.W. Drinkwater, A.M. Quinn, The use of ultrasound in the investigation of rough surface interfaces, J. Tribol-T Asme. 123 (2001) 8–16.
[43] C. Jacq, D. Nelias, G. Lormand, D. Girodin, Development of a three-dimensional semi-analytical elastic-plastic contact code, J. Tribol-T Asme. 124 (2002) 653–667.
[44] P. Sainsot, C. Jacq, D. Nelias, A numerical model for elastoplastic rough contact, Cmes-Comp. Model. Eng. 3 (2002) 497–506.
[45] Z.J. Wang, W.Z. Wang, Y.Z. Hu, H. Wang, A numerical elastic-plastic contact model for rough surfaces, Tribol. T. 53 (2010) 224–238.
[46] G. Liu, Q.J. Wang, C. Lin, A survey of current models for simulating the contact between rough surfaces, Tribol. T. 42 (1999) 581–591.
[47] F.P. Bowden, D. Tabor, The Friction and Lubrication of Solids, Clarendon Press ; Oxford University Press, Oxford; New York, 2008.
[48] J.A. Greenwood, J.B. Williamson, Contact of nominally flat surfaces, in: Proc R Soc Lon Ser-A 295, 1966, 300−+.
[49] F.M. Borodich, Introduction to Zhuravlev's historical paper: on the question of theoretical justification of the Amontons-Coulomb law for friction of unlubricated surfaces, P I Mech. Eng. J-J Eng. 221 (2007) 893–895.
[50] C.H. Lee, M. Eriten, A.A. Polycarpou, Application of elastic-plastic static friction models to rough surfaces with asymmetric asperity distribution, J. Tribol-T Asme. (2010) 132.
[51] N. Yu, A.A. Polycarpou, Combining and contacting of two rough surfaces with asymmetric distribution of asperity heights, J. Tribol-T Asme. 126 (2004) 225–232.
[52] J.F. Archard, Elastic deformation and the Laws of friction, Proc. R Soc. Lon. Ser-A. 243 (1957) 190–205.
[53] R.L. Jackson, J.L. Streator, A multi-scale model for contact between rough surfaces, Wear. 261 (2006) 1337–1347.
[54] B. Bhushan, A. Majumdar, Elastic-plastic contact model for bifractal surfaces, Wear. 153 (1992) 53–64.
[55] A. Majumdar, B. Bhushan, Role of fractal geometry in roughness characterization and contact mechanics of surfaces, J. Tribol-T Asme. 112 (1990) 205–216.
[56] A. Majumdar, B. Bhushan, Fractal model of elastic-plastic contact between rough surfaces, J. Tribol-T Asme. 113 (1991) 1–11.
[57] B.N.J. Persson, Elastoplastic contact between randomly rough surfaces, Phys. Rev. Lett. 87 (2001).
[58] B.N.J. Persson, F. Bucher, B. Chiaia, Elastic contact between randomly rough surfaces: Comparison of theory with numerical results, Phys. Rev. B (2002) 65.
[59] Y.T. Feng, T. Zhao, J. Kato, W. Zhou, Towards stochastic discrete element modelling of spherical particles with surface roughness: a normal interaction law, Comput. Method. Appl. M. 315 (2017) 247–272.
[60] T. Zhao, J. Kato, Y.T. Feng, Stochastic discrete element modelling of rough particles, Springer Proc. Phys. 188 (2017) 183–191.
[61] K.L. Johnson, K. Kendall, A.D. Roberts, D. Tabor, Surface energy and the contact of elastic solids, Proc. Royal Soc. London A Math. Phys. Sci. 324 (1971) 301–313.
[62] A. Dziugys, B. Peters, An approach to simulate the motion of spherical and non-spherical fuel particles in combustion chambers, Granul. Matter 3 (2001) 231–265.
[63] K.L. Johnson, J.A. Greenwood, An approximate JKR theory for elliptical contacts, J. Phys. D. Appl. Phys. 38 (2005) 1042–1046.
[64] J.J. Wu, Numerical analyses on elliptical adhesive contact, J. Phys. D. Appl. Phys. 39 (2006) 1899–1907.
[65] B. Sumer, C.D. Onal, B. Aksak, M. Sitti, An experimental analysis of elliptical adhesive contact, J. Appl. Phys. 107 (2010).
[66] N.H.M. Zini, M.B. de Rooij, M.B.A. Fadafan, N. Ismail, D.J. Schipper, Extending the double-Hertz model to allow modeling of an adhesive elliptical contact, Tribol. Lett. (2018) 66.
[67] J.A. Greenwood, K.L. Johnson, An alternative to the Maugis model of adhesion between elastic spheres, J. Phys. D. Appl. Phys. 31 (1998) 3279–3290.
[68] W.R. Chang, I. Etsion, D.B. Bogy, An elastic-plastic model for the contact of rough surfaces, J. Tribol-T Asme. 109 (1987) 257–263.
[69] Y.W. Zhao, D.M. Marietta, L. Chang, Closure to "discussion of 'an asperity microcontact model incorporating the transition from elastic deformation to fully plastic flow'" [ASME J. Tribol., 122, No. 2, p. 479 (2000)], J. Tribol-T Asme. 122 (2000) 479–480.
[70] R.L. Jackson, I. Green, A finite element study of elasto-plastic hemispherical contact against a rigid flat, J. Tribol-T Asme. 127 (2005) 343–354.
[71] D. Cohen, Y. Kligerman, I. Etsion, The effect of surface roughness on static friction and junction growth of an elastic-plastic spherical contact, J. Tribol-T Asme. (2009) 131.
[72] L. Li, I. Etsion, F.E. Talke, Elastic-plastic spherical contact modeling including roughness effects, Tribol. Lett. 40 (2010) 357–363.
[73] H. Ghaednia, X.Z. Wang, S. Saha, Y. Xu, A. Sharma, R.L. Jackson, A review of elastic-plastic contact mechanics, Appl. Mech. Rev. 69 (2017).

[74] L. Vu-Quoc, X. Zhang, L. Lesburg, Normal and tangential force-displacement relations for frictional elasto-plastic contact of spheres, Int. J. Solids Struct. 38 (2001) 6455–6489.
[75] N.V. Brilliantov, F. Spahn, J.M. Hertzsch, T. Poschel, Model for collisions in granular gases, Phys. Rev. E 53 (1996) 5382–5392.
[76] J. Krishnasamy, M.J. Jakiela, A method to resolve ambiguities in corner-corner interactions between polygons in the context of motion simulations, Eng. Comput. 12 (1995) 135–144.
[77] G.T. Houlsby, Potential particles: a method for modelling non-circular particles in DEM, Comput. Geotech. 36 (2009) 953–959.
[78] Y.T. Feng, D.R.J. Owen, A 2D polygon/polygon contact model: algorithmic aspects, Eng. Comput. 21 (2004) 265–277.
[79] Y.T. Feng, K. Han, D.R.J. Owen, Energy-conserving contact interaction models for arbitrarily shaped discrete elements, Comput. Method. Appl. M. 205 (2012) 169–177.
[80] X. Lin, T.-T. Ng, Contact detection algorithms for three-dimensional ellipsoids in discrete element modelling, Int. J. Numer. Anal. Methods Geomech. 19 (1995) 653–659.
[81] J.M. Ting, A robust algorithm for ellipse-based discrete element modelling of granular materials, Comput. Geotech. 13 (1992) 175–186.
[82] T.-T. Ng, Numerical simulations of granular soil using elliptical particles, Comput. Geotech. 16 (1994) 153–169.
[83] A. Dziugys, B. Peters, A new approach to detect the contact of two-dimensional elliptical particles, Int. J. Numer. Anal. Methods Geomech. 25 (2001) 1487–1500.
[84] K. Kildashti, K.J. Dong, B. Samali, A revisit of common normal method for discrete modelling of non-spherical particles, Powder Technol. 326 (2018) 1–6.
[85] J. Harkness, Potential particles for the modelling of interlocking media in three dimensions, Int. J. Numer. Methods Eng. 80 (2009) 1573–1594.
[86] H. Fessler, E. Ollerton, Contact stresses in toroids under radial loads, Brit. J. Appl. Phys. 8 (1957) 387–393.
[87] A. Podlozhnyuk, S. Pirker, C. Kloss, Efficient implementation of superquadric particles in discrete element method within an open-source framework, Comput. Part. Mech. 4 (2017) 101–118.
[88] A. Beheshti, M.M. Khonsari, On the contact of curved rough surfaces: contact behavior and predictive formulas, J. Appl. Mech-T Asme. (2014) 81.
[89] R. Jedynak, Exact and approximate solutions of the infinite integrals of the asperity height distribution for the Greenwood-Williamson and the Greenwood-Tripp asperity contact models, Tribol. Int. 130 (2019) 206–215.
[90] N.V. Brilliantov, T. Pöschel, Collision of adhesive viscoelastic particles, Phys. Granular Media (2004) 189–209.
[91] D.S. Goldobin, E.A. Susloparov, A.V. Pimenova, N.V. Brilliantov, Collision of viscoelastic bodies: Rigorous derivation of dissipative force, Eur. Phys. J. E. (2015) 38.
[92] J.M. Hertzsch, F. Spahn, N.V. Brilliantov, On low-velocity collisions of viscoelastic particles, J. Phys. II 5 (1995) 1725–1738.
[93] J. Jamari, D.J. Schipper, Experimental investigation of fully plastic contact of a sphere against a hard flat, J. Tribol-T Asme. 128 (2006) 230–235.
[94] J. Jamari, D.J. Schipper, An elastic-plastic contact model of ellipsoid bodies, Tribol. Lett. 21 (2006) 262–271.
[95] B. Bhushan, Contact mechanics of rough surfaces in tribology: multiple asperity contact, Tribol. Lett. 4 (1998) 1–35.
[96] B. Bhushan, G.S. Blackman, Atomic force microscopy of magnetic rigid disks and sliders and its applications to tribology, J. Tribol-T Asme. 113 (1991) 452–457.
[97] J.I. Mccool, Comparison of models for the contact of rough surfaces, Wear. 107 (1986) 37–60.
[98] Y.R. Jeng, P.Y. Wang, An elliptical microcontact model considering elastic, elastoplastic, and plastic deformation, J. Tribol-T Asme. 125 (2003) 232–240.
[99] L. Vu-Quoc, L. Lesburg, X. Zhang, An accurate tangential force–displacement model for granular-flow simulations: contacting spheres with plastic deformation, force-driven formulation, J. Comput. Phys. 196 (2004) 298–326.
[100] H. Deresiewicz, Oblique contact of nonspherical elastic bodies, J. Appl. Mech. 24 (1957) 623–624.
[101] R.D. Mindlin, H. Deresiewicz, Elastic spheres in contact under varying oblique forces, J. Appl. Mech-T Asme. 20 (1953) 327–344.
[102] A. Faraji, A. Cardou, A. Gakwaya, Effect of arbitrarily directed tangential force on elastic contacting bodies, J. Eng. Mech-Asce. 125 (1999) 1324–1326.
[103] H. Deresiewicz, Mechanics of Granular Matter**This study was supported by the Office of Naval Research under contract Nonr-266(09) with Columbia University, in: H.L. Dryden, T. von Kármán (Eds.), Advances in Applied, Elsevier, Mechanics, 1958, pp. 233–306.
[104] U. Olofsson, L. Hagman, A model for micro-slip between flat surfaces based on deformation of ellipsoidal elastic bodies, Tribol. Int. 30 (1997) 599–603.
[105] T. Hisakado, T. Tsukizoe, Effects of distribution of surface slopes and flow pressures of contact asperities on contact between solid-surfaces, Wear. 30 (1974) 213–227.
[106] H.A. Sherif, S.S. Kossa, Relationship between Normal and tangential contact stiffness of nominally flat surfaces, Wear. 151 (1991) 49–62.
[107] Q.J. Zheng, Z.Y. Zhou, A.B. Yu, Contact forces between viscoelastic ellipsoidal particles, Powder Technol. 248 (2013) 25–33.
[108] J.J. Kalker, Three-dimensional elastic bodies in rolling contact, in: Solid Mechanics and Its Applications, Springer Netherlands, 1990.
[109] P.J. Vermeulen, K.L. Johnson, Contact of nonspherical elastic bodies transmitting tangential forces, J. Appl. Mech. 31 (1964) 338.